Master equation modelling of excitonic loss processes in phosphorescent OLEDs
On the importance of spatial correlations

van Hoesel, Clint

Award date:
2021

Department of Applied Physics
Molecular Materials and Nanosystems
Master Applied Physics, (BIO)NANO Track

Master equation modelling of excitonic loss processes in phosphorescent OLEDs

On the importance of spatial correlations

Clint van Hoesel
1012071

60 ECTS Master Thesis
This Master Thesis was performed conform the TU/e Code of Scientific Conduct
CONFIDENTIAL

Supervisors:
Prof. dr. Peter A. Bobbert
Mahyar Taherpour, MSc.

Committee:
Prof. dr. Peter A. Bobbert
Prof. dr. Reinder Coehoorn
Dr. Wouter G. Ellenbroek
Prof. dr. Jaime Gómez Rivas

Eindhoven, Friday 25th June, 2021

Abstract

Displays based on organic light-emitting diode (OLED) technology are becoming more prevalent due to their numerous advantages, such as power efficiency. As of yet there are some aspects to OLEDs that reduce its versatility. Loss processes of the light-emitting quasiparticles dubbed excitons reduce the power efficiency of OLED devices and enhance the degradation of the materials within the emissive layer. These loss processes within phosphorescent OLEDs (Ph-OLED) consist of the mutual annihilation of triplet excitons and the quenching of a triplet exciton by a polaron. Both these loss processes generally occur as a Förster-type energy transfer interaction, which is dependent on the spatial distance between particles. This gives rise to correlations in the relative positions between the surviving triplets and polarons. Generally only in kinetic monte carlo (KMC) simulations these are properly taking into account, but these can be computationally expensive. Other techniques tend to ignore these spatial correlations. Here we present a method based on the master equation as solved within KMC simulations. Our method is based on the calculation of statistical averages applied to the master equation of an Ph-OLED system, from which a Bogoliubov-Born-Green-Kirkwood-Yvon hierarchy arises. This hierarchy is infinitely long and we will discuss several closures in order to make this finitely long, such that the system of equations can be solved. We compare our results with KMC simulations and prove that our method is an accurate and computationally cheap tool to be used alongside KMC simulations for the modelling of exciton dynamics within Ph-OLEDs. We prove that during transient photoluminescent experiments TTA and TPQ cause a deviation from the exponential radiative decay and quantify this contribution. Furthermore we find during steady-state operation at high current densites that the exciton density grows as a power law where the exponent is lower than one and quantify the generation rate at which the roll-off starts. Lastly we find that the diffusion of exciton and polarons mediates the TTA and TPQ processes and further increases the losses in which that lattice structure plays a vital role and causes percolation effects. In total this work provides valuable insights into the loss of power efficiency and luminance at high current densities as observed in Ph-OLEDs.

Contents

1. Introduction

Organic materials are prevalent throughout (opto-)electronic devices nowadays. Organic materials are taking some of the market away from the traditional inorganic semicoductors, such as silicon and gallium arsenide. Currently organic materials are commercially applied as field-effect transistors [1], solar cells [2] and light-emitting diodes [3]. The organic light-emmiting diode (OLED) technology is especially popular among organic opto-electronics, currently being implemented in the display of a large fraction of flagship smartphones. The Samsung Galaxy S21, Apple iPhone 12 and Google Pixel 5 are among the most prominent current examples. This is caused by the numerous advantages organic semiconductors have over their inorganic counterparts. The term *organic* imples that the materials are generally composed of carbon and hydrogen atoms, but can also consist of other organic atoms and can even contain heavy metals such as iridium. Carbon-based molecules are generally quite cheap, thus these electronics are generally more cost-effective than the traditional inorganic materials. Organic materials tend to be insulators, thus should not be appropriate for electronic devices. In 2000 the Chemical Prize went to Alan J. Heeger, Alan G. MacDiarmid, and Hideki Shirakawa for their work on polymers with conductive properties [4]. Their work and that of many others starting around 1915 [5] on conductive organic materials opened the gateways for organic electronics with equal performance to inorganic electronics. In this work we will focus on the popular OLED technology.

In this chapter we will first discuss the general operation princples of OLEDs (section 1.1). Then we will move on to introducing the dynamics of excitons in OLED structures (section 1.2). Furthemore a small summary of current modelling techniques is presented in section 1.3. Lastly we will outline the reason for this work and what will be discussed in the following chapters in section 1.4.

1.1 Organic light-emitting diodes

Organic materials with (electro)luminescent properties have been studied, since the start of the twentieth century [6]. The work presented in Ref. [7] is widely regarded as the first modern OLED. Their device was an amorphous organic thin film based on Alq_3 and achieved an external quantum efficiency (EQE) of 1%. After this work the technological developments followed very quickly and brought us to the current state of OLED research. This development has brought us displays which have the advantage that the contrast ratio is high [8], have low-power consumption, low cost, can be flexible, thin and support large viewing angles [9], especially when compared to convential display techniques such as LCD. The main disadvantage that remains is the lifetime of OLEDs which is relatively short to other display types due to degradation of the material [10]. This is related to the other main disadvantage of OLEDs, the roll-off of internal quantum efficiency (IQE) at higher current densities. The underlying principles of this roll-off will be the central topic of this thesis.

As noted above OLEDs operate on the principle of converting electricity in light. On a quantum mechanical level this consists of an electron and hole combining into a quasiparticle dubbed exciton which in the ideal world decays radiatively. In order to efficiently accommodate this reaction a complex structure has to be created. One simple example of such an OLED structure is shown in figure 1.1. The y-axis denotes the energy of the energy levels, while the x-axis denotes the depth within the OLED structure, which indicates the different consecutive layers. Note that the high-lying energy levels here denote the lowest unoccupied molecular orbitals (LUMO) energy level, while the low-lying energy levels illustrate the highest occupied molecular orbitals (HOMO) energy level of each individual layer. During active operation a voltage is applied over the cathode to anode. Electrons are injected from the cathode into the electron injection layer (EIL) where they are transported through the hole blocking layer (HBL) into the emissive layer (EML). The holes traverse the reverse direction being injected from the anode into the hole injection layer (HIL) transported through the electron blocking layer (EBL) into

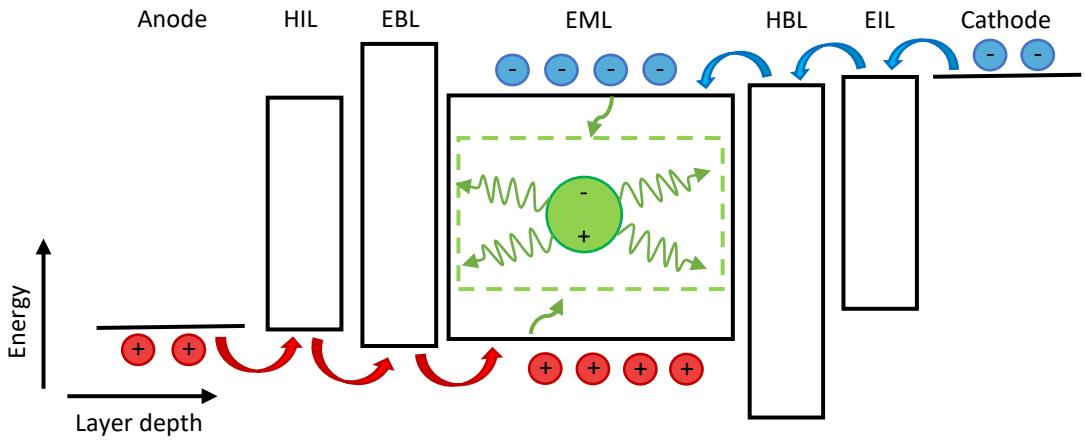

Figure 1.1: Schematic energy diagram of an OLED structure. Electrons (blue) are injected from the cathode into the EIL through the HBL into the EML. They are confined there by the EBL. Holes (red) are injected from the anode into the HIL and transported through the EBL into the EML where they are confined by the HBL. Within the EML the electrons and holes will form excitons (green). The excitons will (generally) decay radiatively.

the EML. In the emissive layer the electrons and holes will form excitons. Generally the EML mostly is made up of a host material with conductive properties and is doped with a guest material with luminescent properties. Usually the HOMO and LUMO of the guest material lay higher and lower respectively than the HOMO and LUMO of the host material as indicated in figure 1.1. The emissive guest thus acts as a trap for the electrons and holes increasing the efficiency of the recombination process. The recombination efficiency is further increased by the confinement of the electrons and holes within the EML by the EBL and HBL respectively. After the formation of the exciton on the guest material, the guest will facilitate the radiative decay.

The properties of these excitons are crucial to the OLED. Since both the electron (e) and hole (h) are spin-1/2 particles, the resulting exciton can be either of singlet- (S) or triplet-type (T) [11]. Under normal conditions only the singlet can decay radiatively due to spin conservation. The exciton formation reaction for randomly spin-polarised electrons and hole is given by [12]

$$(e_\uparrow + e_\downarrow)(h_\uparrow + h_\downarrow) \rightarrow S + 3T. \tag{1.1}$$

Thus only 25% of the excitons are formed as a singlet and can decay on fluorescent materials. This can be increased to 50% or decreased to 0% for anti-parallel or parallel aligned spin polarisation of the electron and hole respectively [12]. In this work we will only look at currents without spin polarisation. In that case the distribution of singlet to triplet is 1 : 3, as is indicated in figure 1.2. The original OLEDs only consisted of fluorescent materials, in which case the theoretical maximum percentage of the electrons converted into photons, referred to as the internal quantum efficiency (IQE), cannot exceed 25%[1], which makes the first generation OLED consume a high amount of electronic energy per photon. Consecutive iterations of OLEDs have alleviated this problem and brought the theoretical obtainable IQE to 100%.

The second generation OLEDs increased their IQE by creating a pathway through which the triplets can decay radiatively [15]. Normally this is spin forbidden, however by the introduction of heavy metals [15, 16] into the molecules, this becomes possible. The heavy metals introduce spin-orbit coupling (SOC) to the molecule. This ensures that the triplet states will not be purely of triplet-nature, but will partially be of singlet-character. This facilitates the spin-flip needed for triplets to decay radiatively. This process is referred to as phosphorescence. Furthermore the SOC facilitates the singlets spin-flipping into the triplet state, which is referred to as intersystem

[1]It has been noted that theoretically a fifth of the triplets can be converted into singlets through TTA [13] (TTA will be discussed later). This would theoretically raise IQE_{max} to 40%.

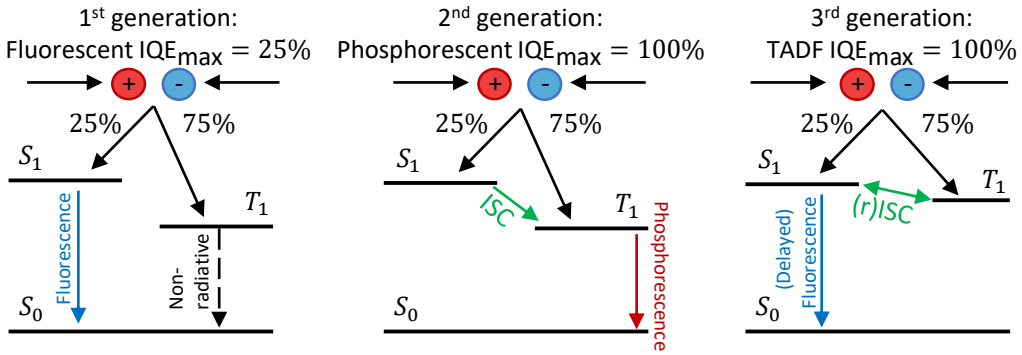

Figure 1.2: Schematic energy level diagram of the lowest singlet and triplet excitonic states with relevant transitions between the excitonic states of the three earliest generations of OLEDs. In all cases the excitons are generated by electrons and holes recombining. Initially for all cases 25% of the excitons will be singlets, while 75% will be triplets. In the first generation only the singlets are able to decay rediatively, while the triplets will not decay radiatively, thus causing the maximum obtainable IQE to be 25%. In the second generation OLEDs singlets are able to convert into triplets through ISC (mediated by SOC). SOC furthermore allows the triplets to decay radiatively, thus the maximum IQE becomes 100%. In the third generation OLEDs triplets are thermally excited and converted into singlets (rISC). The excitons will decay radiatively as singlets. This brings the maximum IQE of the third generation to 100%. Note that in the third generation the difference between singlet and triplet energies (ΔE_{ST}) has to be small in order to allow for rISC. Inspired by Ref. [14].

crossing (ISC). ISC is generally orders of magnitude faster than the radiative decay of a singlet in these materials [17, 18]. This process is sped up by the large difference in energies of the singlet and triplet state (ΔE_{ST}, generally in the order of $2k_BT$ at room temperature [19]). Effectively all excitons formed by the electrons and holes will be triplets before decaying radiatively. This increases the maximum obtainable IQE to 100%. The second generation is referred to as phosphorescent OLEDs (Ph-OLEDs) and will be the main focus of this work.

Further generations are under development, due to heavy metals being rare and thus expensive. Of large academic and commercial interest is thus currently the third generation of OLEDs. Here the spin-orbit coupling should still be present in order to facilitate ISC, but can be much weaker. The main property of this generation is the small difference between singlet and triplet energies ΔE_{ST}. All in all this allows the triplets to be thermally converted into singlets, referred to as reverse intersystem crossing (rISC), instead of radiatively decaying through phosphorescence. Singlets will decay radiatively through fluorescence. A fraction will decay instantly after formation, due to being formed as singlets and not undergoing ISC. The triplets however will first have to be upconverted to singlet before decaying radiatively through fluorescence. The third generation is henceforth referred to as thermally activated delayed fluorescent (TADF) OLEDs [20]. The TADF process increases the maximum IQE to 100%.

The TADF OLEDs do not seem to be the last OLED generation. TADF OLEDs still have an issue with the long lifetime of the triplets which causes degradation of the material. Further research is therefore being conducted into newer generations of OLEDs in order to alleviate this long lifetime of the triplets. For the fourth generation of OLEDs new techniques developed are based on hyperfluorescence [21] and the direct singlet harvesting mechanism [22]. These techniques will not be discussed here, since these are beyond the scope of this work. Very recently work on possibly the fifth generation OLEDs was introduced in Ref. [23]. They have found molecules with a negative singlet-triplet energy gap, such that ISC (not rISC) becomes thermally activated. This could significantly reduce triplet lifetimes.

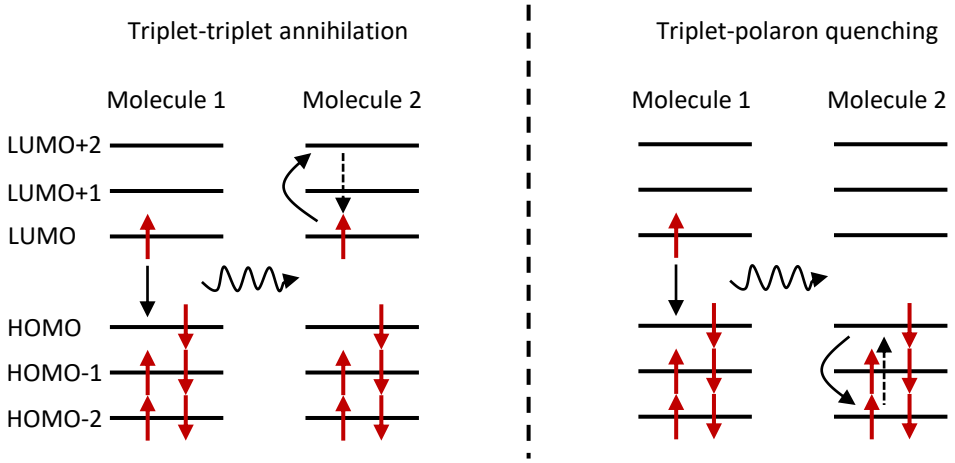

Figure 1.3: Schematic overview of TTA and TPQ loss processes. During TTA one of the triplets recombines. The energy released excites another triplet, either staying a triplet or becoming singlet. The electron in the excited state will trickle down to the LUMO non-radiatively, thus losing the energy of the first triplet non-radiatively. During TPQ again a triplet recombines. This time the energy excites the polaron on molecule 2, in this example the polaron is of positive nature. The polaron then decays non-radiatively to its non-excited state, thus the energy of the triplet is again lost non-radiatively. Inspired by Ref. [26].

1.2 Exciton dynamics

As noted we will focus here on the second generation in which to good approximation all excitons are triplets. Even though the strong SOC allows triplets to decay radiatively, the triplet lifetime is in the order of micro-seconds [24, 25]. This lifetime is high enough for other processes to occur instead. In Ref. [24] the two most significant loss processes were reported. These two processes are schematically presented in figure 1.3.

It has been reported that the most prominent of these two loss processes is triplet-triplet annihilation (TTA) [16, 27] which is plotted on the left in figure 1.3. Generally what happens is that one of the excitons recombines, releasing its energy. This energy is transferred to the other triplet, exciting it electronically and/or vibrationally. Depending on the initial spins of the triplets, during the excitement the second triplet turns into a singlet [26]. Theoretically it is also possible to create an excitonic quintet state on a single molecule, but that generally is higher in energy, thus that pathway is energetically unfavourable [26]. This excited singlet or triplet will tend to non-radiatively decay back into the lowest energy triplet state, following Kasha's rule [28]. In total the system has thus lost the energy of one triplet non-radiatively. In reaction form this is denoted as [26]

$$T_1 + T_1 \rightarrow \begin{cases} S_n^* + S_0 \\ T_n^* + S_0 \end{cases} \rightarrow \begin{cases} S_1 + S_0 + \text{heat} \\ T_1 + S_0 + \text{heat} \end{cases}, \tag{1.2}$$

where S_0 denotes the groundstate and T_n^* denotes an excited triplet. Due to the fact that two excitons are needed for TTA, its contribution to the decay is proportional to n_T^2, where n_T denotes the triplet density in the system.

Depending on the system the triplet-polaron quenching (TPQ) can become the dominant loss process of triplets [27, 29, 30]. TPQ is generally dominant at low current densities, when the amount of triplets is low, since the contribution of TPQ to the loss of excitons scales as n_T. One example of TPQ is depicted in figure 1.3 on the right. Again the triplet decays to the S_0 state, but now transfers its energy to the polaron, in this case a hole, and excites electronically and/or vibrationally. The polaron will then tend to decay non-radiatively to its lower energy level. The energy of the triplet is again lost non-radiatively. The total reaction can be written as [14]

$$P^{\pm} + T_1 \rightarrow P^{\pm *} + S_0 \rightarrow P^{\pm} + S_0 + heat. \tag{1.3}$$

The transfer of the excitonic energy in TTA and TPQ has to be mediated by transfer interactions. The interactions generally taken into account are the Förster-type [31, 32] and Dexter-type [32] energy transfer [19]. The basis of Förster-type interactions are dipole-dipole interactions between molecules. The rate of Förster-type processes are given by [31]

$$k_{Förster}^{\text{Process}}(r) = k_r \left(\frac{R_F^{Process}}{r} \right)^6, \tag{1.4}$$

where k_r is some characteristic timescale, which can be chosen if we appropriately scale $R_F^{Process}$ and which we will set to the inverse radiative lifetime of a triplet on a phosphorescent molecule, r denotes the distance of the energy transfer and $R_F^{Process}$ denotes the characteristic length scale of a specific dipole-dipole-type energy transfer reaction. These processes range from TTA and TPQ to the simple hopping of an exciton over different molecules. Dexter-type energy transfer happens through exchange interactions, which are mediated by the overlap of wavefunctions between the initial and final state. The rate of a Dexter-type process is is equal to [32]

$$k_{Dexter}^{\text{Process}}(r) = k_{D,0}^{Process} e^{-2r/\lambda^{Process}}, \tag{1.5}$$

where $k_{D,0}^{\text{Process}}$ is some characteristic timescale related to the relevant Dexter-type interaction and $\lambda^{Process}$ denotes the localisation length of the specific process and related wavefunctions. The processes again range from TTA and TPQ to the simple hopping of excitons or polarons. Dexter [32] furthermore derived that dipole-quadropole and higher order multipole expansion interactions are also present, but these are generally not considered in the OLED literature, since their effects generally seem to be insignificant.

Comparing these two type of energy transfers we can conclude that at long-range Förster-type processes will always be dominant, due their r^{-6} nature instead of inverse exponential behaviour. It has be shown that both for the hopping of excitons [25] and TTA [33] at distances larger than (approximately) the nearest-neighbour distance Förster-type interactions are dominant. Since excitons generally live on guest sites, which only occupy a small fraction of the total amount of molecules, the average distance between sites is quite large for both TTA and the hopping of excitons, such that these can be approximated purely by Förster-type interactions. For TPQ the main mechanism for energy transfer is as of yet unclear, since polarons will be hopping at a fast rate, possibly allowing for Dexter-type energy transfer to become dominant.

When TTA and TPQ processes occur after a number of hopping steps, it is often referred to as diffusion-mediated multi-step TTA or TPQ. If there are no hopping steps in between to mediate, the loss processes are referred to as single-step TTA and TPQ. Diffusion mediation generally enhances the loss due to TTA and TPQ.

1.3 Modelling of excitonic dynamics

As has been noted in many works [14, 34, 35] the modelling of OLEDs spans multiple length and time scales. On the macroscale the physics of the complete OLED device is modelled. Here the dynamics of charges hopping, dynamics of excitons and light outcoupling play an important role. These three processes are however affected by the underlying morphology on the mesoscale, which gives rises to effects such as percolation. Going down even further to the microscale we find that density functional theory (DFT) becomes the norm for the quantum mechanical determination of energy transfer rates.

In this thesis we will focus on modelling exciton dynamics somewhere in between the meso- and device scale. Multiple techniques already exist and will be discussed below. We will add our novel method to this collection.

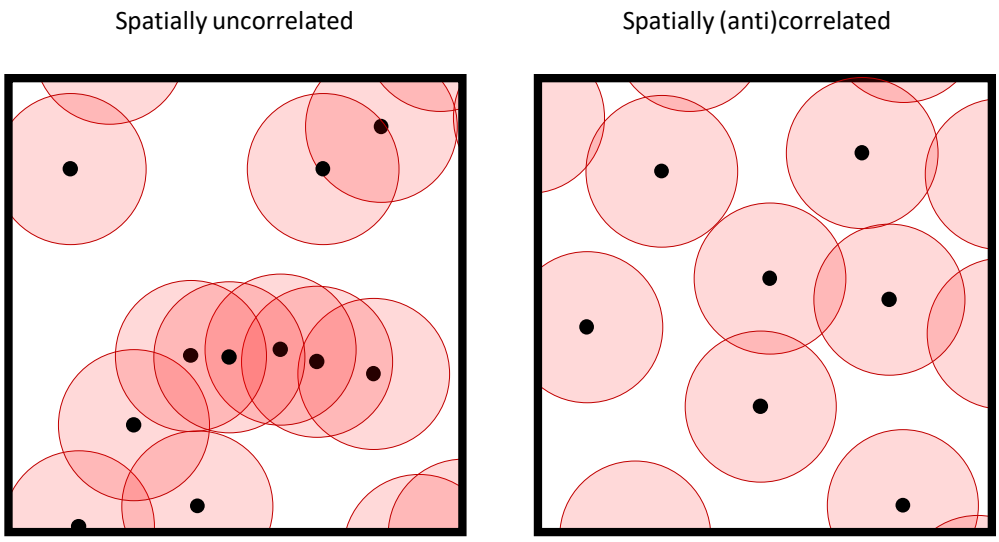

Figure 1.4: Illustration of correlation effects on the positioning of excitons throughout an EML. The black dots indicate excitons and the red circle indicates the Förster radius around it. On the left excitons are randomly distributed, which corresponds to the initial condition of exciton distribution for a TRPL experiment. On the right the positions of excitons are spatially anticorrelated, as is caused by TTA without hopping of excitons. The correlated positions were modelled using equation (2.24). Inspired by Ref. [37].

1.3.1 Mean-field modelling

As early as the discovery of TTA in Ph-OLEDs mean-field modelling (also referred to as rate equations) has been applied in order to bring to light its loss processes [16]. Such a phenomenological model of TTA is generally given by [16]

$$\frac{n_T(t)}{dt} = Gn_{max} - k_r n_T(t) - \frac{k_{TTA}}{2} n_T^2(t), \tag{1.6}$$

where G denotes the generation rate, n_{max} the density of guest sites, k_r denotes the radiative decay rate of the triplet excitons and k_{TTA} is the TTA rate coefficient. The solution to this equation is given in equation (2.19). It has been noted however that this neglects spatial correlation effects caused by the TTA process [36]. This effect is illustrated in figure 1.4. Equation (1.6) will always presume that we are in the situation of the left namely that excitons are completely uncorrelated. As can be concluded the excitons (black) will have more overlap of their Förster-spheres (red) in the uncorrelated case than in the (anti-)correlated situation, thus the TTA effect is more prominent for spatially uncorrelated excitons. Generally TTA operates on excitons which are close to each other, thus the only excitons left after some time will generally be far away from each other, such that the situation on the right is more physically accurate. We can conclude that this method does not give a physically correct solution if excitons do not diffuse, even though it is widely used throughout literature.

1.3.2 Kinetic monte carlo

Another widely used modelling technique of OLEDs is the kinetic monte carlo (KMC) algorithm [29, 36, 38, 39]. The state-of-the-art software Bumblebee [40] will be used to compare our results to. The KMC algorithm allows for modelling any OLED device including spatial correlations. The main drawback of this general algorithm is the fact that simulations can become time-consuming in order to get sufficient statistical accuracy. An extensive introduction to the KMC algorithm applied to OLED modelling can be found in Ref. [34].

1.3.3 Master equation modelling

The last widely used modelling technique is master equation modelling. Formally in this modelling technique probabilities are assigned to any state the system can be in and transition rates are defined between states of the system. This leads continuous-time Markov chains, which need to be solved. In general this is computionally expensive and thus not probabilities of the entire system are evaluated, but the probabilities of states of the individual sites on the lattice[41–43]. This takes into account more spatial correlations than the mean-field modelling, since it can account for percolation effects, but does not take into account all correlations present in the OLED. It terms of accuracy it is thus better than mean-field modelling, but not as accurate as KMC.

Recently a paper was published [44] on charge transport which took this mean-field master equation approach, but added n-particle correlation functions. These higher order correlations become important when particles interact with each other between different sites. In their example these correlations could arise from simple Coulombic interactions between electrons. It was noted however that Coulombic interactions are not needed in order to give rise to these correlations between occupancies [44]. When these n-particle correlation functions are added a Bogoliubov-Born-Green-Kirkwood-Yvon (BBGKY) hierarchy of equations will arise[45–48], which exactly solves the master equation when the correlation order is taken to be the size of the system. This is computationally unfeasible however and these hierarchy need to be closed at relatively small correlation order, such that only a computationally feasible number of equations have to be solved.

1.3.4 Smoluchovski equations

The last relevant technique consists of Smoluchovski equations. As noted above generally spatial correlations are neglected in mean-field modelling, however Smoluchovski equations can describe this spatial decorrelation between particles including Brownian motion [49–51]. These equations are generally given by [50–52]

$$\frac{\partial g_2(r,t)}{\partial t} = \frac{D}{r^2}\frac{\partial}{\partial r}\left(r^2 e^{-U(r)}\frac{\partial}{\partial r}\left(e^{U(r)} g_2(r,t)\right)\right) - S_R(r)\, g_2(r,t)\,, \tag{1.7}$$

where $g_2(r,t)$ is the two particle correlation function, D denotes the diffusion coefficient, $U(r)$ symbolises the interaction potential between particles and $S_R(r)$ denotes the reaction rate at a relative distance between particles r. Based on the two-particle distribution the TTA rate can be adapted. One of the main advantages of this equations, is its simplicity and elegance, allowing for more transparency.

1.4 Outline thesis

As noted all current modelling techniques have their drawbacks. The mean-field modelling techniques generally ignore spatial or occupational correlations and thus yield inaccurate results. KMC does solve the complete master equation of the system, but it can be time-consuming to get sufficient accuracy and it may be difficult to draw conclusion from the overabundance of data. As such there is need for an accurate and fast technique for the modelling of exciton dynamics including spatial correlations, applicable to amorphous structures.

In this thesis we will attempt to create such a modelling technique. Since master equations are capable of modelling an entire OLED system we will start there. Solving the master equation directly is computionally infeasible, we will follow the previous literature and calculate the moments of occupancies [44]. This will net us with a BBGKY hierarchy of equations. We will bring this hierarchy of equations from a discrete lattice into a continuum definition as is suitable for the generally amorphous [7, 26] OLED structures and allows for simpler analytical formulas, getting close to a Smoluchovski equation. Then we will close the BBGKY infinitely long hierarchy of equations by applying closures influenced by Refs. [44, 53] and one of our own.

In chapter 2 we will introduce the master equation of the exciton within a system. Here we will perform the

steps outlined above. We will also attempt to model a system including polarons and compare our diffusion modelling to Fick's second diffusion law. In chapter 3 we will present the results of the model we have created. We will furthermore discuss these results and compare them to the results from KMC simulations. Finally in chapter 4 we will summarise and conclude the chapters previous to it and provide an outline for further research.

2. Theory

In this chapter the mathematical and computational methods will be discussed pertaining to the modelling of triplets in an emission layer of a Ph-OLED. Part of this chapter can also be found in Ref. [37]. First in section 2.1 we will present our model simulating exciton dynamics, where we will step from a master equation approach to a BBGKY-hierarchy of equations. This hierarchy of equations will need to be closed before we can solve it. This closure will be discussed in section 2.2. For certain closures this system cannot be solved analytically. In section 2.3 we will discuss the numerical solving method used for solving the integro-differential equations. Furthermore in section 2.4 we will add polarons to this system and add the TPQ loss process. Lastly in section 2.5 we will discuss the relation of our integral hopping formulation to the Smoluchovski equation, which is more common in continuum formulations. Throughout this chapter we will make use of *Mathematica* [54] in order to solve complex integrals and differential equations analytically.

2.1 General model

We consider a system with an arbitrary amount of points distributed throughout space. These points represent the molecules and will be referred to as sites from now on. These sites are capable of being occupied by one or zero excitons ($n_i \in \{0,1\}$ with n_i being the amount of excitons at site i). All excitons can be assumed to be triplets due to the rate of intersystem crossing generally being significantly faster than the other relevant time scales in phosphorescent emitting OLED layers [17]. We define the set of all sites $\mathcal{I}$. The system has 2^N configurations where $N\,(=|\mathcal{I}|)$ is the amount of sites. Each configuration has occupations $(n_1,\ldots,n_N)$. Since we generally do not know what configuration the system is in, we assign a probability to every valid configuration $P\,(n_1,\ldots,n_N)$. The modelling of this system then turns into a continuous time-Markov chain, here referred to as master equation.

The rates of the master equation depend on the physics of the system. Here I will assume the same physical processes within a 2$^{\text{nd}}$ generation OLED emitting layer as Ref. [37], namely:

- Decay of excitons. It will be assumed that the only contribution to direct decay is from spontaneous radiative decay, but it is a simple exercise to add non-radiative decay to these simulations. Generally it will be assumed that the radiative decay rate $k_r(=\frac{1}{\tau})$ is equal to 1 μs^{-1}, which is inline with observed decay rates for a couple of phosphorescent emitters [17, 24, 25]. Generally this will be the characteristic timescale and all other timescales will be made dimensionless to k_r where possible.

- Hopping of excitons with rate D_{ij}, where $i,j \in \mathcal{I}$. According to theoretical computations in a host-guest system at low guest percentage Förster-type is dominant [25], thus we will assume that the hopping rate can be written as

$$D_{i,j} = k_r \left(\frac{R_{F,Diff}}{\Delta r_{ij}}\right)^6, \tag{2.1}$$

  where $R_{F,Diff}$ denotes the Förster radius of the hopping process in relation to k_r and Δr_{ij} denotes $|\boldsymbol{r}_j - \boldsymbol{r}_i|$. Note that $D_{ij} = D_{ji}$, since it is assumed that energy disorder can be neglected, yielding symmetric diffusion rates. For guest emitters of the same type then it has been found that $R_{F,Diff} \approx 1.5$ nm [25], whereas $R_{F,Diff}$ can be up to 4 nm for molecules of a different type [55].

- Generation of excitons. An empty site will be able to generate an exciton with rate G. The generation rate is assumed to be completely uniform throughout space. This mathematical form of generation of excitons captures excitation by light or recombination of electrons and holes as long as there is no spatial

dependency on the generation rate. This generally holds within the bulk of the material or directly at the interface between layers.

- Triplet-triplet annihilation. As introduced in chapter 1 two triplets near each other can undergo a reaction where one triplet is lost non-radiatively as shown in equation (1.2). At larger distances the Förster-type energy transfer dominates the TTA process [33]. Since in host-guest systems the average distance between guest sites are on average larger than the distance at which Förster-type becomes dominant [33], it is fair to assume that TTA only occurs as a Förster-type process. Thus we can write

$$W_{i,j} = k_r \left(\frac{R_{F,TTA}}{\Delta r_{ij}} \right)^6 , \tag{2.2}$$

where $R_{F,TTA}$ denotes the Förster radius of the TTA process where the rate of losing either one of the excitons equals $2k_r$, in agreement with the original definition in equation (1.4) as presented in Ref. [31]. Note that the Förster radius to lose either one of the excitons with a rate of k_r has an extra factor $2^{1/6}$. Generally $R_{F,TTA}$ will be assumed to be in the order of 3 nm in correspondence with other comparisons of simulations with experiments [56].

Due to the physical processes outlined above the probabilities of each configuration evolve through time. We can then put this in a classical master equation, assuming coherent quantum effects can be neglected, given by [37]

$$\begin{aligned} \frac{dP\left(n_1,\ldots,n_N,t\right)}{dt} = & \sum_{i\in\mathcal{I}} \sum_{j\in\mathcal{I}\setminus i} \left[-W_{i,j} n_i n_j P\left(n_1,\ldots,n_N,t\right) + W_{i,j} n_i \left(1-n_j\right) P\left(\ldots,n_j+1,\ldots,t\right) \right. \\ & \left. - D_{i,j} n_i \left(1-n_j\right) P\left(n_1,\ldots,n_N,t\right) + D_{i,j} n_j \left(1-n_i\right) P\left(\ldots,n_i+1,\ldots,n_j-1,\ldots,t\right) \right] \\ & + \sum_{i\in\mathcal{I}} \left[-k_r n_i P\left(n_1,\ldots,n_N,t\right) + k_r \left(1-n_i\right) P\left(\ldots,n_i+1,\ldots,t\right) \right. \\ & \left. - G\left(1-n_i\right) P\left(n_1,\ldots,n_N,t\right) + G n_i P\left(\ldots,n_i-1,\ldots,t\right) \right] . \end{aligned} \tag{2.3}$$

The first line outlines the transition rates due to TTA, the second line represents the hopping rate of triplet excitons, the third line denotes the radiative decay of triplet excitons and the last line indicates the generation of triplets. This equation can be translated into the very simple equation $\frac{d\boldsymbol{p}(t)}{dt} = \boldsymbol{A}\,\boldsymbol{p}\left(t\right)$, where $\boldsymbol{p}(t)$ denotes the vector of probabilities of all possible configuration and the matrix $\boldsymbol{A}$ denotes the transition rates between the states. This equation has the restriction that at any time t the sum of all probabilities should equal 1 ($\mathbf{1}^T\boldsymbol{p}(t) = 1$), thus $\frac{d}{dt}\left(\mathbf{1}^T\boldsymbol{p}(t)\right) = 0 = \mathbf{1}^T\boldsymbol{A}\boldsymbol{p}(t)$. This is equivalent to saying that the sum of all elements in all columns of matrix $\boldsymbol{A}$ should sum to 0. We can conclude from equation (2.3) that this holds. This has the simple solution $\boldsymbol{p}\left(t\right) = \exp\left(\boldsymbol{A}\left[t-t_0\right]\right)\boldsymbol{p}\left(t_0\right)$[57], where $\boldsymbol{p}\left(t_0\right)$ denotes the initial probabilities. It is not feasible computationally to use this very simple solution in order to model actual OLED systems. The amount of non-zero elements in matrix $\boldsymbol{A}$ grows as $2^N\left(\frac{N[N+1]}{2}+1\right)$. This means that an ordinary computer will not be able to carry out this computation for $N \gtrapprox 35$ due to memory constraints, while in order to model actual OLED systems one generally needs N to be in the order of 10^3 or higher.

In order to be able to model large systems we will be calculating the statistical averages of excitonic occupation of sites, the evolution of which is described by the master equation (2.3). Then the application of symmetries will allow us to model infinitely large systems. First we choose a subset of sites $\mathcal{I}_{corr} \subset \mathcal{I}$ of $N_{corr}\,(=|\mathcal{I}_{corr}|)$ sites. Then we determine the discrete N_{corr}-particle correlation function as

$$\overline{\prod_{i\,\in\mathcal{I}_{corr}} n_i}\,(t) = \left(\prod_{j\in\mathcal{I}} \sum_{n_j\in\{0,1\}} \right) \left(\prod_{i\in\mathcal{I}_{corr}} n_i \right) P\left(n_1,\ldots,n_N,t\right), \tag{2.4}$$

where $\overline{A}(t)$ denotes the average value of the general observable A at time t. Note that we assume that all elements in $\mathcal{I}_{corr}$ are unique, however all these derivations also hold for subsets with duplicate elements, since from equation (2.4) it follows that $\overline{n_i^2 A} = \overline{n_i A}$. Now calculating the time derivative of equation (2.4) and plugging this into equation (2.3) yields

$$\begin{aligned}\frac{d}{dt}\overline{\prod_{i\in\mathcal{I}_{corr}} n_i}(t) &= \left(\prod_{j\in\mathcal{I}}\sum_{n_j\in\{0,1\}}\right)\left(\prod_{i\in\mathcal{I}_{corr}} n_i\right)\frac{\partial}{\partial t}P(n_1,\ldots,n_N,t)\\ &= -\overline{\prod_{i\in\mathcal{I}_{corr}} n_i}\left(|\mathcal{I}_{corr}|\,[G+k_r] + \sum_{j\in\mathcal{I}_{corr}}\sum_{k\in\mathcal{I}_{corr}\setminus j} W_{j,k}\right) - \sum_{j\in\mathcal{I}\setminus\mathcal{I}_{corr}}\sum_{k\in\mathcal{I}_{corr}} W_{j,k}\overline{n_j\prod_{i\in\mathcal{I}_{corr}} n_i}\\ &\quad + G\sum_{j\in\mathcal{I}_{corr}}\overline{\prod_{i\in\mathcal{I}_{corr}\setminus j} n_i} + \sum_{j\in\mathcal{I}_{corr}}\sum_{k\in\mathcal{I}\setminus\mathcal{I}_{corr}} D_{j,k}\left(\overline{n_k\prod_{i\in\mathcal{I}_{corr}\setminus j} n_i} - \overline{\prod_{i\in\mathcal{I}_{corr}} n_i}\right),\end{aligned} \tag{2.5}$$

where $|\mathcal{I}_{corr}|$ denotes the amount of particles in $\mathcal{I}_{corr}$ (N_{corr}). One important fact to note in equation (2.5) is that the time dependence of the N_{corr}-particle correlation function is dependent on the $N_{corr}+1$-correlation function. This means that we have found an hierarchy of N differential equations, much like the Bogoliubov-Born-Green-Kirkwood-Yvon (BBKGY) [45–48] hierarchy of equations. It is generally not feasible to perform the ODE calculations of the hierarchy of N equations, especially in the limit of $N\to\infty$. Thus closures will be needed in order to be able to solve this problem. The closures will be discussed further in section 2.2.

Equation (2.5) gives the time evolution of the correlation between N_{corr} discrete sites. This would leave us in total with $\sum_{N_{Corr}=1}^{N_{cutoff}}\binom{N}{N_{corr}}$ correlation functions, where N_{cutoff} denotes the degree of correlation at which a cutoff is applied. In the case of $N\to\infty$ this quickly becomes insurmountable even when N_{cutoff} is small. One approach as outlined in [37] is to assume a periodic lattice, such as a simple cubic lattice and apply symmetries such as translational symmetry and C_4 rotational symmetry (cubic lattice point symmetry groups). This assumes that the system has a periodic lattice which is generally not true for emitting OLED layers, which are amorphous in nature [19, 26].

Here we employ another method of solving theses system of equation by going to a continuum formulation of the N_{corr}-particle correlation function

$$\begin{aligned}\tilde{\tilde{g}}_{N_{corr}}(\boldsymbol{r}_1,\ldots,\boldsymbol{r}_{N_{corr}},t) &= \left(\prod_{j=1}^{N_{corr}}\frac{1}{\delta V_j}\int_{\delta V_j} d\tilde{\boldsymbol{r}}_j^3\right)\\ &\quad \sum_{\mathcal{I}_{corr}\subset\mathcal{I},\,|\mathcal{I}_{corr}|=N_{corr}}\left(\overline{\prod_{i\in\mathcal{I}_{corr}} n_i}(t)\prod_{i\in\mathcal{I}_{corr}}\sum_{j=1}^{N_{corr}}\delta(\tilde{\boldsymbol{r}}_{\boldsymbol{j}}-\boldsymbol{r}_{\boldsymbol{i}})\right),\end{aligned} \tag{2.6}$$

where δV_j denotes a small volume around $\boldsymbol{r}_j$. What we are doing in this equation is defining N_{corr} volumes δV_j situated around the positions $(\boldsymbol{r}_1,\ldots,\boldsymbol{r}_{N_{corr}})$. Then we determine whether there are sites within those volumes and determine the N_{corr}-exciton correlation function between sites in the different volumes δV_j and average those over the volumes. Next step is to reduce the complexity by applying symmetries. Due to neglecting energy disorder and assuming that the system is infinitely large, we can conclude that all interesting physics is only relative to other particles. We can thus average over the position of the first particle, since that degree of freedom will provide no information. We can thus calculate the spatially averaged N_{corr}-particle correlation function as

$$\tilde{g}_{N_{corr}}\left(\boldsymbol{r}_2,\ldots,\boldsymbol{r}_{N_{corr}},t\right)=\left(\frac{1}{V}\int_V d\tilde{\boldsymbol{r}}_1^3\right)\left(\prod_{j=2}^{N_{corr}}\frac{1}{\delta V_j}\int_{\delta V_j} d\left(\tilde{\boldsymbol{r}}_j-\tilde{\boldsymbol{r}}_1\right)^3\right) \sum_{\mathcal{I}_{corr}\subset\mathcal{I},\,|\mathcal{I}_{corr}|=N_{corr}}\left(\overline{\prod_{i\in\mathcal{I}_{corr}} n_i}\left(t\right)\prod_{i\in\mathcal{I}_{corr}}\sum_{j=1}^{N_{corr}}\delta\left(\tilde{\boldsymbol{r}_j}-\tilde{\boldsymbol{r}}_1-\boldsymbol{r_i}\right)\right), \tag{2.7}$$

where V is the volume of the system, which will generally be very large. We can then furthermore set δV_j very small, allowing us to operate at excellent fidelity. Note that the degrees of freedom for $N_{corr}>2$ are equal to $3N_{corr}-6$, when assuming spherical symmetry.

Now calculating the time derivative of the spatially averaged N_{corr}-particle correlation function and employing equation (2.5) yields

$$\begin{aligned}
&\frac{\partial}{\partial t}\tilde{g}_{N_{corr}}\left(\boldsymbol{r}_2,\ldots,\boldsymbol{r}_{N_{corr}},t\right)\\
&=-\tilde{g}_{N_{corr}}\left(\boldsymbol{r}_2,\ldots,\boldsymbol{r}_{N_{corr}},t\right)\left(N_{corr}\left[G+k_r\right]+\sum_{i=1}^{N_{corr}}\sum_{j=i+1}^{N_{corr}}2W\left(\boldsymbol{r}_i,\boldsymbol{r}_j\right)\right)\\
&\quad-\int_V d\mu^3\left(\boldsymbol{r}_2,\ldots,\boldsymbol{r}_{N_{corr}+1}\right)\sum_{k=1}^{N_{corr}}W\left(\boldsymbol{r}_{N_{corr}+1},\boldsymbol{r}_k\right)\tilde{g}_{N_{corr}+1}\left(\boldsymbol{r}_2,\ldots,\boldsymbol{r}_{N_{corr}+1},t\right)\\
&\quad+n_{max}\sum_{k=1}^{N_{corr}}G\tilde{g}_{N_{corr}-1}\left(\boldsymbol{r}_2,\ldots,\boldsymbol{r}_{k-1},\boldsymbol{r}_{k+1},\ldots,\boldsymbol{r}_{N_{corr}},t\right)\\
&\quad+n_{max}\int_V d\mu^3\left(\boldsymbol{r}_2,\ldots,\boldsymbol{r}_{N_{corr}+1}\right)\sum_{k=1}^{N_{corr}}D\left(\boldsymbol{r}_{N_{corr}+1},\boldsymbol{r}_k\right)\left[\tilde{g}_{N_{corr}}\left(\boldsymbol{r}_2,\ldots,\boldsymbol{r}_{k-1},\boldsymbol{r}_{k+1},\ldots,\boldsymbol{r}_{N_{corr}+1},t\right)\right.\\
&\qquad\qquad\left.-\tilde{g}_{N_{corr}}\left(\boldsymbol{r}_2,\ldots,\boldsymbol{r}_{N_{corr}},t\right)\right],
\end{aligned} \tag{2.8}$$

where the product of Dirac delta functions has been replaced by $d\mu(\boldsymbol{r})$ denoting the distribution function of sites as function of space. We have defined n_{max} as the average density of sites, which is related to the maximum exciton density.

In order to proper model the system, we will be systematically plugging in higher values for N_{corr}. Starting with $N_{corr}=1$, which is actually the exciton density of the system $\tilde{g}_1\left(t\right)=n_T\left(t\right)$, we retrieve from equation (2.8)

$$\begin{aligned}
\frac{dn_T\left(t\right)}{dt}=&\frac{d\tilde{g}_1\left(t\right)}{dt}\\
=&-\int_V d\mu^3\left(\boldsymbol{r}_2\right)W\left(\boldsymbol{r}_2\right)\tilde{g}_2\left(\boldsymbol{r}_2,t\right)-\left[k_r+G\right]n_T\left(t\right)+Gn_{max}\\
=&-n_T^2\left(t\right)\int_V\mu\left(d\boldsymbol{r}_2^3\right)W\left(\boldsymbol{r}_2\right)g_2\left(\boldsymbol{r}_2,t\right)-\left[k_r+G\right]n_T\left(t\right)+Gn_{max},
\end{aligned} \tag{2.9}$$

where $g_{N_{corr}}\left(\boldsymbol{r}_2,\ldots,\boldsymbol{r}_{N_{corr}}\right)$ is defined as the normalised N_{corr}-particle correlation function $\frac{\tilde{g}_{N_{corr}}(\boldsymbol{r}_2,\ldots,\boldsymbol{r}_{N_{corr}},t)}{n_T^{N_{corr}}(t)}$. The normalised N_{corr}-particle correlation function provides more transparent insight into the physics and will be used for the rest of this work. The next step is to calculate the time-dependence of $g_2(\boldsymbol{r}_2,t)$ yielding

$$\begin{aligned}\frac{dg_2(\boldsymbol{r}_2,t)}{dt} =& -n_T(t)\int d\mu^3(\boldsymbol{r}_2,\boldsymbol{r}_3)\,g_3(\boldsymbol{r}_2,\boldsymbol{r}_3,t)\left[W(\boldsymbol{r}_3)+W(\boldsymbol{r}_3-\boldsymbol{r}_2)\right]\\ &+2n_T(t)\,g_2(\boldsymbol{r}_2,t)\int d\mu^3(\boldsymbol{r}_3)\,g_2(\boldsymbol{r}_3,t)\,W(\boldsymbol{r}_3)\\ &-2g_2(\boldsymbol{r}_2,t)\left(W(\boldsymbol{r}_2)+\frac{Gn_{max}}{n_T(t)}\right)+2\frac{Gn_{max}}{n_T(t)}\\ &+n_{max}\int d\mu^3(\boldsymbol{r}_2,\boldsymbol{r}_3)\left\{D(\boldsymbol{r}_3)\left[g_2(\boldsymbol{r}_3-\boldsymbol{r}_2,t)-g_2(\boldsymbol{r}_2,t)\right]+D(\boldsymbol{r}_3-\boldsymbol{r}_2)\left[g_2(\boldsymbol{r}_3,t)-g_2(\boldsymbol{r}_2,t)\right]\right\}.\end{aligned} \tag{2.10}$$

In this entire thesis we will not go further than the two-particle correlation function (also called pair correlation function). This is analysed to third order in Ref. [37].

Comparing equation (2.9) to the mean-field (rate) equation (1.6) it can be shown that

$$k_{TTA}(t) = 2\int_V d\mu^3(\boldsymbol{r}_2)\,W(\boldsymbol{r}_2)\,g_2(\boldsymbol{r}_2,t). \tag{2.11}$$

The next step is to define the distribution of sites $d\mu^3(\boldsymbol{r})$. The 2-site distribution function $\mu(r)$ is equal to the radial distribution function. For amorphous systems the radial distribution function is complex, but generally resembles $\mathrm{rdf}(r) \approx 1+\frac{\phi(r)}{r}$ for infinitely large systems at large distances [58]. The materials within OLED emissive layers seem to adhere to this relation as shown in Ref. [59]. In order to generate simple expressions we will be assuming that $\phi(r)=0$. Furthermore we will be assuming that the distribution of the third site can be separated into three terms only consisting of the relative positions between two sites. This yields for the distribution of sites

$$\mu(\boldsymbol{r}) = \begin{cases}1 & \text{if } |\boldsymbol{r}| \geq R_0\\ 0 & \text{else}\end{cases}, \tag{2.12}$$

$$d\mu^3(\boldsymbol{r}_2) = \mu(\boldsymbol{r}_2)\,d\boldsymbol{r}_2^3, \tag{2.13}$$

$$d\mu^3(\boldsymbol{r}_2,\boldsymbol{r}_3) = \mu(\boldsymbol{r}_3)\,\mu(\boldsymbol{r}_3-\boldsymbol{r}_2)\,d\boldsymbol{r}_3^3. \tag{2.14}$$

In section 3 we will compare this method to KMC simulations on a cubic lattice. A cubic lattice has a different radial distribution function and higher order site distribution function than we use as given in the equations above. In order to get comparable result, we set R_0, such that the TTA rates without any correlations are equal $n_{max}\int_V \mu\left(d\boldsymbol{r}_2^3\right)W(\boldsymbol{r}_2) = \sum_i W_{0,i}$. Assuming that the summation happens over a simple cubic lattice with Förster-type TTA, this yields

$$\frac{4\pi}{3R_0^3} \approx \frac{8.402}{a^3}, \tag{2.15}$$

where we used $n_{max} = \frac{1}{a^3}$, with a the cubic lattice spacing. This yields $R_0 = 0.7929a$. Generally a is set to 1 nm in KMC simulations as it is close to experimental values of actual OLED molecules [59].

Furthermore in order to be able to model the hierarchy of equations as given by equations (2.9) and (2.10), we need boundary conditions. It is assumed that both at at $t=0$ over all space and at large distances between pairs of sites for all time t the excitons are completely uncorrelated. This yields the boundary conditions

$$n_T(0) = n_0, \tag{2.16}$$
$$g_2(r, 0) = 1, \tag{2.17}$$
$$\lim_{r\to\infty} g_2(r, t) = 1. \tag{2.18}$$

Here we have furthermore defined the initial triplet density as n_0.

2.2 Closures

The last problem keeping us from solving the equations (2.9) and (2.10) is the fact that $g_3(\boldsymbol{r}_2, \boldsymbol{r}_3, t)$ is unknown. We do not want to continue the hierarchy of equations above $N_{corr} = 2$ in this work. Therefore we need to make an assumption for $g_3(\boldsymbol{r}_2, \boldsymbol{r}_3, t)$ with only known variables in order to close the system of equations. The assumption should be based on physical principles [60] valid within the system. In this section we will present and discuss several closures of the hierarchy of equations.

2.2.1 Negligible covariance closure

One of the simplest ways of cutting off the hierarchy found in literature is to assume that higher order covariances (of order N_{cutoff} and higher) are negligible as proposed in Ref. [44]. In practice this means setting $\overline{\prod_{i\in\mathcal{I}_{N_{cutoff}}} \delta n_i} = \overline{\prod_{i\in\mathcal{I}_{N_{cutoff}}} (n_i - \overline{n_i})} = 0$. This closure, the negligible covariance closure (NCC), approximates reality when decorrelation effects are stronger than (anti)correlation effects for N_{cutoff} or higher particle correlation functions. In this problem that is specifically the case when $R_{F,Diff} \gg R_{F,TTA}$ or when $G \gg k_r \left(\frac{R_{F,TTA}}{R_0}\right)^6$. For $N_{cutoff} = 2$ we find $g_2(\boldsymbol{r}_2, t) = 1$. Using the boundary condition (2.18), we also find $g_2(\boldsymbol{r}_2, t) = 1$ if $D(\boldsymbol{r}_2) \to \infty$ from equation (2.10). Then we only need to solve equation (2.9) with the analytical solution

$$n_T(t) = \frac{1}{k_{TTA}} \left(\sqrt{(G+k_r)^2 + 2Gk_{TTA}n_{max}} \tanh\left(\tanh^{-1}\left(\frac{G + k_r + k_{TTA}n_0}{\sqrt{(G+k_r)^2 + 2Gk_{TTA}n_{max}}} \right) + \frac{1}{2} t \sqrt{(G+k_r)^2 + 2Gk_{TTA}n_{max}} \right) - G - k_r \right), \tag{2.19}$$

where $k_{TTA} = \frac{8k_r\pi R_{F,TTA}^6}{3R_0^3}$. Note that in this case (2.9) was equal to (1.6). We will call this the first order NCC closure, which is the same as the mean-field modelling. In the case of $G = 0$ we retrieve the well-known equation[16]

$$n_T(t) = \frac{k_r n_0}{e^{k_r t}\left(k_r + \frac{k_{TTA}}{2}n_0\right) - \frac{k_{TTA}}{2}n_0}. \tag{2.20}$$

Lastly in the case of $t \to \infty$ we find

$$n_{T,eq} = \frac{\sqrt{(G+k_r)^2 + 2Gk_{TTA}n_{max}} - k_r - G}{k_{TTA}}. \tag{2.21}$$

Applying the NCC closure at $N_{cutoff} = 3$ yields $g_3(\boldsymbol{r}_1, \boldsymbol{r}_2, \boldsymbol{r}_3) = g_2(\boldsymbol{r}_1, \boldsymbol{r}_2) + g_2(\boldsymbol{r}_1, \boldsymbol{r}_3) + g_2(\boldsymbol{r}_2, \boldsymbol{r}_3) - 2$, but it is only possible to solve the system numerically with this closure. We will call this the second order NCC closure. Notice that for this closure it is possible that $g_3(\boldsymbol{r}_1, \boldsymbol{r}_2, \boldsymbol{r}_3) < 0$ when the sum $g_2(\boldsymbol{r}_1, \boldsymbol{r}_2) + g_2(\boldsymbol{r}_1, \boldsymbol{r}_3) + g_2(\boldsymbol{r}_2, \boldsymbol{r}_3) < 2$, which is unphysical. In chapter 3 we do see that this situation is observed (figure 3.2).

2.2.2 Kirkwood superposition closure

Another well-known closure is the Kirkwood superposition approximation closure (KSC) [53]. It is given by

$$g_3(\boldsymbol{r}_1, \boldsymbol{r}_2, \boldsymbol{r}_3) = g_2(\boldsymbol{r}_1, \boldsymbol{r}_2)\, g_2(\boldsymbol{r}_1, \boldsymbol{r}_3)\, g_2(\boldsymbol{r}_2, \boldsymbol{r}_3). \tag{2.22}$$

This form is quite elegant and easy to work with. It states that the three particle correlation function is a simple multiplication of the three independent two particle correlation functions. This is expected to do well, since the only term consists of all correlations between two particles and there are no direct interactions between three particles in this physical system.

It has been noted within the theory of fluids that this closure is not complete and the right side of equation (2.22) has to be multiplied by a factor $S_3(\boldsymbol{r}_1, \boldsymbol{r}_2, \boldsymbol{r}_3, n_T) = e^{-\frac{W_3(\boldsymbol{r}_1, \boldsymbol{r}_2, \boldsymbol{r}_3, n_T)}{k_B T}}$, where $W_3(\boldsymbol{r}_1, \boldsymbol{r}_2, \boldsymbol{r}_3, n_T)$ is the indirect mean force [61]. It has been derived for low densities that this correction term is given by $S_3(\boldsymbol{r}_1, \boldsymbol{r}_2, \boldsymbol{r}_3, n_T) = 1 + n_T \int d\boldsymbol{r}_4 h(\boldsymbol{r}_4 - \boldsymbol{r}_1)\, h(\boldsymbol{r}_4 - \boldsymbol{r}_2)\, h(\boldsymbol{r}_4 - \boldsymbol{r}_3) + O\left(n_T^2\right)$[61, 62], where $h(\boldsymbol{r}) = g_2(\boldsymbol{r}) - 1$. From this we can conclude in the limit of zero exciton density that the SPC is the ground truth. Furthermore it has been proven that when entropy is maximised the Kirkwood superposition closure is the ground truth [63]. In general OLEDs operate at low exciton densities, such that the Kirkwood superposition approximation is close to reality. We can only solve the system of equations numerically with this closure.

2.2.3 Pair approximation

It can be noted that both equations (2.9) and (2.10) have terms of different order in n_T. OLEDs generally operate at low exciton densites, such that the terms of higher order in the triplet density can be ignored. This allows us to ignore the higher order correlation terms by taking the limit of $n_T \to 0$ and thus the hierarchy of equations is closed. We will call this limit cutoff when applied at $N_{corr} = 2$ the pair approximation closure (PA), since the third particle in the system is not taken into account.

Taking the limit of low exciton density ($n_T \to 0$) within equation (2.9) leads to the trivial equation

$$n_T(t) = \left(n_0 - \frac{G n_{max}}{k_r + G}\right) e^{-(k_r + G)t} + \frac{G n_{max}}{k_r + G}, \tag{2.23}$$

which only holds if $n_T(t)$ is orders of magnitude smaller than $4\pi \int_{R_0}^{\infty} r^2 W(r)\, g_2(r, t)$ $\left(\leq \frac{4\pi R_{F,TTA}^6}{3R_0^3}\right)$ at any time t (note $\frac{G n_{max}}{k_r + G} \leq n_T(t) \leq n_0$ if $n_0 \geq \frac{G n_{max}}{k_r + G}$, otherwise the order is reversed). This is identical to assuming TTA does not occur in the system.

This limit can also be applied to the derivative of the two particle correlation function in equation (2.10). In order to then generate exact formulas we will split the simulation into two different situations.

Transient photoluminescence

In transient photoluminescence (TRPL) experiments the system starts with exciton triplets scattered throughout the system and which will start decaying. In this case there is no further generation of triplets, thus $G = 0$. In

the limit of low exciton density then in equation (2.10) we can ignore the three particle correlation function. Assuming that excitons are perfectly confined to their sites $D_{i,j} = 0$ then the solution to equation (2.10) is

$$g_2(r,t) = g_2(r,0)\, e^{-2tW(r)}, \tag{2.24}$$

as has been found before in literature [49]. Note that here $W(r)$ is still completely general and can be a mix of both Förster- and Dexter-type TTA. We can conclude that a correlation hole is created with radius $R_{corr,Forster} \propto R_{F,TTA}\,(k_r t)^{1/6}$ or $R_{corr,Dexter} \propto \lambda_{Dex} \ln(k_{Dex} t)$ respectively. In TRPL experiment it is assumed that excitons start out spatially uncorrelated as assumed before in equation (2.17). It can then be derived for Förster-type TTA that

$$\begin{aligned}\int_V \mu\left(d\boldsymbol{r}_2^3\right) W(\boldsymbol{r}_2)\, g_2(\boldsymbol{r}_2,t) &= \sqrt{\frac{2}{k_r t}}\frac{\pi R_{F,TTA}^3}{3}\left(\sqrt{\pi} - \Gamma\left(\frac{1}{2}, \frac{2R_{F,TTA}^6 k_r t}{R_0^6}\right)\right) \\ &= \frac{k_{TTA}(t)}{2},\end{aligned} \tag{2.25}$$

where $\Gamma(x,t)$ denotes the upper incomplete Gamma function. For $t \gg \frac{R_0^6}{2R_{F,TTA}^6 k_r}$ we can approximate with a high degree of accuracy $R_0 = 0$. The fraction $\frac{R_0^6}{2R_{F,TTA}^6}$ is generally in the order of 10^{-4}. Now plugging this into equation (2.9) yields

$$n_T(t) = \frac{n_0 e^{-k_r t}}{1 + \frac{\sqrt{2}}{3}\pi^2 n_0 R_{F,TTA}^3 \operatorname{erf}\left(\sqrt{k_r t}\right)}, \tag{2.26}$$

where $\operatorname{erf}(x)$ is the error function. This equation has already been found in literature before in Ref. [39], where we have found that $b = \frac{1}{\sqrt{2}}$, which is very close to their fitted parameter $b = 0.71$. Other literature generally has a different factor than $\sqrt{2}$, such as 1 [64], which could be related to an alternative definition of the Förster-radius as noted earlier.

Above we have analysed the OLED system in the case of three spatial dimensions. There exist OLED structures where the majority of the excitons live on the interface between layers. In these cases it might be interesting to evaluate hierarchy of equations for two spatial dimensions or even fractal spatial dimensions. In that case we can simply replace $4\pi \int_{R_0}^{\infty} dr r^2$ by the d-dimensional integral $\frac{2\pi^{d/2}}{\Gamma(d/2)} \int_{R_0}^{\infty} dr r^{d-1}$. Replacing this integral in equation (2.9) yields the solution

$$n_T(t) = \frac{n_0 e^{-k_r t}}{1 + \frac{2^{d/6}}{6\Gamma(d/2)} n_0 \pi^{d/2} R_{F,TTA}^d \Gamma(1 - d/6)\, \gamma(d/6, k_r t)}, \tag{2.27}$$

where $\gamma(x,t)$ denotes the lower incomplete Gamma function. This allows us to evaluate systems with one or two spatial dimensions as well. Note that the unit of both $n_T(t)$ and n_0 has now become length^{-d}.

Steady state

The other case in which we can get analytical solutions is the steady state. During steady state operation the generation of excitons due to either charges or photons counteract the radiative decay of the exctions and TTA.

In steady state we will use the fact that in any equation $\frac{\partial}{\partial t} = 0$ holds. In that case we can derive for the two particle correlation function from equation (2.10)

$$g_2(r, G) = \frac{1}{1 + \frac{W(r) n_{T,eq}(G)}{G n_{max}}}. \tag{2.28}$$

Again $W(r)$ is completely general and can be either Förster- or Dexter-type TTA. We again find a correlation hole with size $R_{corr,\text{Förster}} = R_{F,TTA}\left(\frac{k_r n_{T,eq}}{G n_{max}}\right)^{1/6}$ or $R_{corr,Dexter} = \lambda \ln\left(\frac{k_{Dex} n_{T,eq}}{G n_{max}}\right)$. Now assuming that Förster-type TTA is the dominant process, we find that effective TTA rate has become $k_{TTA}(G) = \frac{4\pi^2}{3} R^3_{F,TTA} \sqrt{\frac{k_r G n_{max}}{n_{T,eq}(G)}}$. With these results we can rewrite equation (2.9) in the steady state as

$$G n_{max} = (k_r + G) n_{T,eq}(G) + \frac{2\pi^2}{3} R^3_{F,TTA} n^{3/2}_{T,eq}(G) \sqrt{k_r G n_{max}}. \tag{2.29}$$

This yields a cubic equation, which can be solved analytically, but that solution will not be presented here. Instead a simplified piecewise function can be derived

$$n_{T,eq}(G) \approx \begin{cases} G n_{max}/k_r & \text{if } G \leq k_r \min\left(1,\ \left(\frac{2}{3}\pi^2 R^3_{F,TTA} n_{max}\right)^{-1}\right) \\ n_{max} & \text{if } G \geq k_r \max\left(1,\ \left(\frac{2}{3}\pi^2 R^3_{F,TTA} n_{max}\right)^{2}\right) \\ \left(\frac{G}{k_r} n_{max}\right)^{1/3} \left(\frac{2\pi^2}{3} R^3_{F,TTA}\right)^{-2/3} & \text{otherwise} \end{cases}. \tag{2.30}$$

Assuming that $G n_{max} \approx \frac{J}{el}$, we have derived at which current density TTA will become dominant and the electron to photon conversion will see diminishing returns. Here J is the current density and l is the width of the device. Note that here we have taken the limit of $R_0 \to 0$, which holds if $R^6_{corr} \gg R^6_0$. This condition is violated at high generation rates G. We can also conclude that at low generation values k_{TTA} remains constant as was also found in Ref [65]. In d spatial dimensions this becomes

$$G n_{max} = (k_r + G) n_{T,eq}(G) + \frac{k_r^{d/6} (G n_{max})^{1-d/6} \pi^{1+d/2}}{\Gamma(d/2) \sin\left(d\frac{\pi}{6}\right)} R^d_{F,TTA} n^{1+d/6}_{T,eq}(G). \tag{2.31}$$

This equation is valid for $0 < d < 6$. Note that in the intermediate regime the steady-state exciton density in other spatial dimensionalities is given by $n_{T,eq}(G) = (G n_{max}/k_r)^{\frac{d}{6+d}} \left(\frac{\Gamma(d/2)\sin\left(d\frac{\pi}{6}\right)}{\pi^{1+d/2} R^d_{F,TTA}}\right)^{\frac{6}{6+d}} \propto G^{\frac{d}{6+d}}$.

2.3 Finite element method

In the sections above we have discussed all necessary ingredients in order to be able to solve equations (2.9) and (2.10). Aside from the analytical results found in the sections above, no analytical solutions were found. This leaves solving this system of equations numerically. The main problem here is discretising $g_2(r, t)$ in the spatial direction.

We will be employing a finite element method, based on the Galerkin method [66]. First of all we employ separation of variables. This allows us to rewrite the two particle correlation function as $g_2(r, t) = \sum_{i=1}^{N_{bf}} \alpha_i(t) u_i(r)$,

where N_{bf} denotes the number of basis functions. This method works best if the basis functions resemble the exact solution.

In order to now actually numerically solve this system we calculate the time derivative of the inner product between the m^{th} basis function and $g_2(r,t)$ yielding

$$\left(u_m, \frac{\partial g_2}{\partial t}\right) = \sum_{i=1}^{N_{bf}} (u_m, u_i) \frac{d\alpha_i(t)}{dt}, \tag{2.32}$$

where $\frac{\partial g_2(r,t)}{\partial t}$ is still given by equation (2.10). The inner product will be defined as $(f,g) = \int_0^\infty dr f(r) g(r)$. This problem can be simplified by choosing orthonormal basis functions $(u_i, u_j) = \delta_{ij}$. We will choose simple basis functions given by

$$u_i(r) = \begin{cases} \frac{1}{\sqrt{r_{bf,i+1} - r_{bf,i}}} & \text{if } r_{bf,i} \leq r < r_{bf,i+1} \\ 0 & \text{else} \end{cases}, \tag{2.33}$$

where $r_{bf,i}$ denotes the i^{th} boundary radius. These boundary radii will be set to $r_{bf,i} = e^{\ln(R_0) + \frac{\ln(R_{max}) - \ln(R_0))}{N_{bf}}(i-1)}$. Here I have introduced a new parameter R_{max}, which denotes the maximum distance at which g_2 will be evaluated. This then changes the boundary condition (2.18) to $g_2(R_{max}, t) = 1$ for any time t. R_{max} will be set to a radius, such that the difference between the new boundary condition and boundary condition (2.18) is negligible.

This allows us to rewrite equation (2.32) using equation (2.10) as

$$\frac{d}{dt}\alpha_a(t) = \boldsymbol{T}_a^{bcd}\alpha_b\alpha_c\alpha_d + \boldsymbol{U}_a^{bc}\alpha_b\alpha_c + \boldsymbol{V}_a^b\alpha_b + \boldsymbol{W}_a, \tag{2.34}$$

where the Einstein summation convention was used. Here the tensors consist of the integrals in $\left(u_m, \frac{\partial g_2}{\partial t}\right)$. All elements of the tensors in equation (2.34) contain integrals. These integrals will be calculated numerically using either simple Gaussian quadratures [67] or when the integrand is complex the enhanced VEGAS algorithm [68, 69]. For the SPC closure we will need all tensors shown above, thus the computational time and memory needed grow as $O\left(N_{bf}^4\right)$. For the pair approximation we only need $\boldsymbol{V}_a^b$ and lower, which grows as $O\left(N_{bf}^2\right)$. The pair approximation will computationally be much cheaper than SPC for high amounts of basis functions.

2.4 Inclusion of triplet-polaron quenching

The model as described in section 2.1 only inlcudes the triplet-triplet annihilation loss process. The significant loss process of excitons at low current densities, triplet-polaron quenching (TPQ), was ignored. In this section we will add TPQ to the model.

We keep the arbitrarily spatially distributed sites, but now these sites can also be occupied by a polaron such that $n_i \in \{0, T, P\}$. We then add the following physical processes to this system

- Hopping of polarons. Polarons can generally hop over both guests and hosts. In that case hopping can be assumed to be mostly caused by the overlap of wavefunctions which can be written as

$$D_{i,j}^{PP} = k_{hop} e^{-2\frac{r}{\lambda}}, \tag{2.35}$$

where k_{hop} denotes the rate of hopping at no distance and λ is the localized length. Generally λ is at least 0.1 nm[25].

- Triplet-polaron quenching. A polaron and triplet near each other can react. This reaction generally occurs as described in equation (1.3). It is still under discussion whether Dexter-or Förster-type transfer is dominant for the TPQ process. This likely depends on the hopping rate of polarons. In the case of trap-limited hopping likely Förster-type TPQ is dominant, since the average reaction distance will be higher, such that it is fair to write

$$W_{i,j}^{TPQ} = k_r \left(\frac{R_{F,TPQ}}{\Delta r_{ij}} \right)^6, \tag{2.36}$$

where generally $R_{F,TPQ} \sim 3$–4 nm [70].

Notice that polarons are not lost nor generated and thus the polaron density will stay constant $n_P(t) = n_P$. Thus the generation as described in section 2.1 will not accurately describe generation due to polarons. Notice that we have also ignored any interaction between polarons such as Coulombic interactions, such that $g_{2,PP} = 1$, where $g_{2,PP}$ is the polaron-polaron two particle correlation function.

These new adaptations allow us to go through the motions of setting up the master equation, applying the method of moments and calculating the normalised correlation functions. The new master equation is presented in the Appendix in equation (A.1). Doing this allows us to rewrite equation (2.9) with TPQ as

$$\begin{aligned} \frac{dn_T(t)}{dt} &= G\left(n_{max} - n_T(t) - n_P\right) - K_{RD} n_T(t) \\ &\quad - \int d\mu^3(\boldsymbol{r}_2) \left(W^{TTA}(r_2)\, n_T^2(t)\, g_{2,TT}(r_2,t) + n_T(t)\, n_P W^{TPQ}(r_2)\, g_{2,TP}(r_2,t) \right), \end{aligned} \tag{2.37}$$

where $g_{2,TP}(r_2,t)$ denotes the triplet-polaron two-particle correlation function. From this equation we can conclude that $k_{TPQ} = \int d\mu^3(\boldsymbol{r}_2)\, W^{TPQ}(r_2)\, g_{2,TP}(r_2,t)$. Note that $n_T(t) + n_P \leq n_{max}$ has to hold at any time t. The time evolution of the triplet-triplet two-particle correlation function then becomes

$$\begin{aligned} \frac{dg_{2,TT}(\boldsymbol{r}_2,t)}{dt} = &- \int d\mu^3(\boldsymbol{r}_2,\boldsymbol{r}_3) \left\{ n_T(t)\, g_{3,TTT}(\boldsymbol{r}_2,\boldsymbol{r}_3,t) \left[W^{TTA}(\boldsymbol{r}_3) + W^{TTA}(\boldsymbol{r}_3 - \boldsymbol{r}_2) \right] \right. \\ &\left. + n_P(t)\, g_{3,TTP}(\boldsymbol{r}_2,\boldsymbol{r}_3,t) \left[W^{TPQ}(\boldsymbol{r}_3) + W^{TPQ}(\boldsymbol{r}_3 - \boldsymbol{r}_2) \right] \right\} \\ &+ 2(t)\, g_{2,TT}(\boldsymbol{r}_2,t) \int d\mu^3(\boldsymbol{r}_2,\boldsymbol{r}_3) \left\{ n_T g_{2,TT}(\boldsymbol{r}_3,t)\, W^{TTA}(\boldsymbol{r}_3) + n_P g_{2,TP}(\boldsymbol{r}_3,t)\, W^{TPQ}(\boldsymbol{r}_3) \right\} \\ &- 2 g_{2,TT}(\boldsymbol{r}_2,t)\, W^{TTA}(\boldsymbol{r}_2) + \frac{2G}{n_T(t)} \left(n_{max} \left[1 - g_{2,TT}(\boldsymbol{r}_2,t) \right] + n_P \left[g_{2,TT}(\boldsymbol{r}_2,t) - g_{2,TP}(\boldsymbol{r}_2,t) \right] \right) \\ &+ 2 \int d\mu^3(\boldsymbol{r}_2,\boldsymbol{r}_3)\, D^{TT}(\boldsymbol{r}_3) \left[n_{max} \left\{ g_{2,TT}(\boldsymbol{r}_3 - \boldsymbol{r}_2, t) - g_{2,TT}(\boldsymbol{r}_2,t) \right\} \right. \\ &\left. + n_P \left\{ g_{3,TTP}(\boldsymbol{r}_2,\boldsymbol{r}_3,t) - g_{3,PTT}(\boldsymbol{r}_2,\boldsymbol{r}_3,t) \right\} \right]. \end{aligned} \tag{2.38}$$

From equation (2.37) we conclude that also the triplet-polaron two-particle correlation function as a function of time needs to be calculated. The time evolution is described as

$$\begin{aligned}\frac{dg_{2,TP}(\boldsymbol{r}_2,t)}{dt} = &-\int d\mu^3(\boldsymbol{r}_2,\boldsymbol{r}_3)\left\{n_T(t)\,g_{3,TPT}(\boldsymbol{r}_2,\boldsymbol{r}_3,t)\,W^{TTA}(\boldsymbol{r}_3)+n_P(t)\,g_{3,TPP}(\boldsymbol{r}_2,\boldsymbol{r}_3,t)\,W^{TPQ}(\boldsymbol{r}_3-\boldsymbol{r}_2)\right\}\\ &+g_{2,TP}(\boldsymbol{r}_2,t)\int d\mu^3(\boldsymbol{r}_2,\boldsymbol{r}_3)\left\{n_T(t)\,g_{2,TT}(\boldsymbol{r}_3,t)\,W^{TTA}(\boldsymbol{r}_3)+n_P g_{2,TP}(\boldsymbol{r}_3,t)\,W^{TPQ}(\boldsymbol{r}_3)\right\}\\ &-g_{2,TP}(\boldsymbol{r}_2,t)\,W^{TPQ}(\boldsymbol{r}_2)+\frac{2G}{n_T(t)}\left(n_{max}\left[1-g_{2,TP}(\boldsymbol{r}_2,t)\right]+n_P\left[g_{2,TP}(\boldsymbol{r}_2,t)-g_{2,PP}(\boldsymbol{r}_2,t)\right]\right)\\ &+\int d\mu^3(\boldsymbol{r}_2,\boldsymbol{r}_3)\Big(D^{TT}(\boldsymbol{r}_3)\left[n_{max}\left\{g_{2,TP}(\boldsymbol{r}_3-\boldsymbol{r}_2,t)-g_{2,TP}(\boldsymbol{r}_2,t)\right\}\right.\\ &\qquad\left.+n_P\left\{g_{3,TPP}(\boldsymbol{r}_2,\boldsymbol{r}_3,t)-g_{3,PPT}(\boldsymbol{r}_2,\boldsymbol{r}_3,t)\right\}\right]\\ &\qquad+D^{PP}(\boldsymbol{r}_3)\left[n_{max}\left\{g_{2,TP}(\boldsymbol{r}_3-\boldsymbol{r}_2,t)-g_{2,TP}(\boldsymbol{r}_2,t)\right\}\right.\\ &\qquad\left.+n_T(t)\left\{g_{3,PTT}(\boldsymbol{r}_2,\boldsymbol{r}_3,t)-g_{3,TTP}(\boldsymbol{r}_2,\boldsymbol{r}_3,t)\right\}\right]\Big).\end{aligned} \tag{2.39}$$

Notice that we have now three-particle correlation functions of different type. Due to the fact that polaron densities are generally quite low in OLED systems [41], we can employ the Kirkwood superposition approximation closure $g_{3,XYZ}(\boldsymbol{r}_1,\boldsymbol{r}_2,\boldsymbol{r}_3)=g_{2,XY}(\boldsymbol{r}_1,\boldsymbol{r}_2)\,g_{2,XZ}(\boldsymbol{r}_1,\boldsymbol{r}_3)\,g_{2,YZ}(\boldsymbol{r}_2,\boldsymbol{r}_3)$, where $X,Y,Z\in\{T,P\}$.

In certain limits we can again derive analytical solutions. These limits will be discussed below.

Strong exciton diffusion

In the case of strong exciton diffusion ($D^{TT}(r)\to\infty$) using boundary condition (2.18) it can be derived from equations (2.38) and (2.39) that $g_{2,TT}(r,t)=1=g_{2,TP}(r,t)$. In that case the solution is a simple adaptation of equation (2.19) yielding

$$\frac{k_{TTA}n_T(t)+k_{single,loss}}{k_{multi,loss}}=\tanh\left(\tanh^{-1}\left(\frac{k_{single,loss}+k_{TTA}n_0}{k_{multi,loss}}\right)+\frac{1}{2}k_{multi,loss}t\right), \tag{2.40}$$

where we have simplified the equations using $k_{single,loss}=G+k_r+k_{TPQ}n_P$ and defined $k_{multi,loss}=\sqrt{(k_{single,loss})^2+2Gk_{TTA}n_{max}}$ with the TPQ rate per polaron density $k_{TPQ}=\frac{4\pi k_r R^6_{F,TPQ}}{3R^3_0}$. Note that in the limit of no polarons in the system ($n_P\to 0$) we retrieve equation (2.19) as should be the case.

Fast polaron hopping

In the case of strong polaronic diffusion ($D^{PP}(r)\to\infty$) $g_{2,TP}(t)=1$. Here we will now again split the solution for either TRPL or steady-state experiments.

During TRPL experiments we again find in the low exciton density limit that $g_{2,TT}$ is given by equation (2.24). Then the solution of equation (2.37) becomes

$$n_T(t)=n_0e^{-k_rt(1+k_{TPQ}n_P)}\left(1+\frac{\sqrt{2}n_0\pi^2R^3_{F,TTA}}{3\sqrt{1+k_{TPQ}n_P}}\operatorname{erf}\left(\sqrt{k_rt\,(1+k_{TPQ}n_P)}\right)\right)^{-1}. \tag{2.41}$$

In steady state $g_{2,TT}$ can be derived from equation (2.38) to be equal to equation (2.28), but we need to replace n_{max} by $n_{max}-n_P$. The solution to be solved in steady state then becomes

$$G\,(n_{max}-n_P)=(k_r+G+k_{TPQ}n_P)\,n_{T,eq}+\frac{2\pi^2}{3}R^3_{F,TTA}n^{3/2}_{T,eq}\sqrt{k_rGn_{max}}. \tag{2.42}$$

No diffusion

The last scenario in which we can obtain exact results is when none of the particles is allowed to diffuse and both the exciton and polaron density is low. This scenario gives a good approximation when k_r is higher than the hopping rate of any particle.

In the case we are simulating TRPL experiments, we find again that $g_{2,TT}$ is given by equation (2.39). From equation (2.39) we can derive that

$$g_{2,TP}(r,t) = g_{2,TP}(r,0)\, e^{-tW^{TPQ}(r)}. \tag{2.43}$$

Plugging this into equation (2.37) gives the solution

$$\begin{aligned} n_T(t) = {} & n_0 e^{-t\left(k_r + n_P k_{TPQ,nd}/\sqrt{k_r t}\right)} \\ & \left(1 + \frac{\sqrt{2}}{3} n_0 \pi^2 R_{F,TTA}^3 e^{k_{TPQ,nd}^2 n_P^2/\left(4k_r^2\right)} \left[\operatorname{erf}\left(k_{TPQ,nd} n_P/k_r + \sqrt{k_r t}\right) - \operatorname{erf}\left(k_{TPQ,nd} n_P/k_r\right)\right]\right)^{-1}, \end{aligned} \tag{2.44}$$

where $k_{TPQ,nd} = \frac{2}{3} k_r \pi^{3/2} R_{F,TPQ}^3$. From this we can conclude that the TTA process becomes irrelevant relatively to the TPQ process when $k_{TPQ,nd} n_P \gg 1$. In words TPQ completely dominates when there are multiple polarons per volume of a sphere with radius $R_{F,TPQ}$.

Now for the steady state first equation (2.39) needs to be solved, yielding

$$g_{2,TP,eq}(r) = \frac{1}{1 + \frac{n_{T,eq} W^{TPQ}(r)}{G(n_{max} - n_P)}}. \tag{2.45}$$

Next this solution is employed in order to solve equation (2.38) yielding

$$g_{2,TT,eq}(r) = \frac{1}{\frac{G(n_{max} - n_P)}{G(n_{max} - n_P g_{2,TP,eq}(r))} + \frac{n_{T,eq} W^{TTA}(r)}{G(n_{max} - n_P g_{2,TP,eq}(r))}}. \tag{2.46}$$

Finally plugging the two particle correlation functions into equation (2.37) yields the equation to be solved

$$\begin{aligned} G(n_{max} - n_P) = {} & n_{T,eq}(G + k_r) + \frac{2}{3}\pi^2 n_P R_{F,TPQ}^3 \sqrt{G k_r n_{T,eq}(n_{max} - n_P)} \\ & + \frac{2}{3}\pi^2 \sqrt{\frac{G k_r n_{T,eq}^3}{n_{max} - n_P}} R_{F,TTA}^3 \left(n_{max} - n_P \frac{R_{F,TTA}^3}{R_{F,TTA}^3 + R_{F,TPQ}^3}\right). \end{aligned} \tag{2.47}$$

2.5 Relation to Smoluchovski equation

In the section above we have used integrals in order to represent the hopping or diffusion of particles in continuum. In general in continuum modelling diffusion is presented as derivatives with regards to spatial coordinates. One example of this was already presented in the Smoluchovski equation (1.7). In this section we will compare these 2 representations of diffusion.

If we assume that particles can do nothing but hop from site to site and ignore the previously assumed uniform distribution of triplets throughout space then from equation (2.5) we can derive for the exciton occupation per site i

$$\frac{dn_i(t)}{dt} = \sum_{j\in\mathcal{I}} D_{ij}\left(n_j(t) - n_i(t)\right) \tag{2.48}$$

or as a continuum representation

$$\begin{aligned}\frac{\partial n(\boldsymbol{r}_1,t)}{\partial t} &= n_{max}\int_V d\boldsymbol{r}_2^3 D(\boldsymbol{r}_2-\boldsymbol{r}_1)\left(n(\boldsymbol{r}_2,t)-n(\boldsymbol{r}_1,t)\right)\\ &= n_{max}\int_V d\boldsymbol{\Delta}^3 D(\boldsymbol{\Delta})\left(n(\boldsymbol{r}_1+\boldsymbol{\Delta},t)-n(\boldsymbol{r}_1,t)\right).\end{aligned} \tag{2.49}$$

Applying the vectorized Taylor expansion, we obtain a Kramers-Moyal expansion in higher dimensionality [71] given by

$$\begin{aligned}\frac{\partial n(\boldsymbol{r}_1,t)}{\partial t} &= n_{max}\int_V d\boldsymbol{\Delta}^3 D(\boldsymbol{\Delta})\sum_{|i|=1}^{\infty}\frac{\boldsymbol{\Delta}^i}{j!}\left(\partial_i n\right)(\boldsymbol{r}_1,t)\\ &= \sum_{|i|=1}^{\infty}\boldsymbol{M}^i\left(\partial_i n\right)(\boldsymbol{r}_1,t),\end{aligned} \tag{2.50}$$

where $\boldsymbol{M}^i = n_{max}\int_V d\boldsymbol{\Delta}^3 D(\boldsymbol{\Delta})\frac{\boldsymbol{\Delta}^i}{j!}$. Notice that when only $|i|=2$ gives a non-zero contribution, we find the first term of the Smoluchovski equation (1.7), which on its own is also known as Fick's second law of diffusion

$$\begin{aligned}\frac{\partial n(\boldsymbol{r}_1,t)}{\partial t} &= \boldsymbol{M}^{\alpha\beta}\frac{\partial}{\partial x^\alpha \partial x^\beta}\left(n(\boldsymbol{r}_1,t)\right)\\ &= D\nabla^2 n(\boldsymbol{r}_1,t).\end{aligned} \tag{2.51}$$

The derivatives we have been considering only have radial components. For respectively Förster- and Dexter-type diffusion the radial components are

$$\begin{aligned}\boldsymbol{M}^{r^i,F} &= 2\pi\int_0^\pi d\theta\sin(\theta)\cos^i(\theta)\int_{R_0}^\infty dr n_{max}\frac{r^{2+i}k_r R_{F,diff}^6}{i!\,r^6}\\ &= \frac{2\left(1+(-1)^i\right)k_r n_{max}\pi R_{F,Diff}^6}{(3-i)\,R_0^{3-i}\,(i+1)!},\end{aligned} \tag{2.52}$$

$$\begin{aligned}\boldsymbol{M}^{r^i,D} &= 2\pi\int_0^\pi d\theta\sin(\theta)\cos^i(\theta)\int_{R_0}^\infty dr n_{max} r^{2+i}\frac{k_{hop}}{i!}e^{2\frac{R_0-r}{\lambda}}\\ &= \frac{\left(1+(-1)^i\right)k_{hop}n_{max}\pi\lambda^{3+i}\Gamma\left(3+i,2\frac{R_0}{\lambda}\right)}{2^{2+i}e^{-2\frac{R_0}{\lambda}}\,(i+1)!}.\end{aligned} \tag{2.53}$$

While the moment of displacement of diffusion drops quickly with higher order i for Dexter-type hopping, for Förster-type hopping the moment of displacement becomes infinitely large for $i \geq 3$. Fickian diffusion is thus unlikely to properly model Förster-type hopping. From these equations we can however conclude that the spherical diffusion constant is equal to

$$D_F = \boldsymbol{M}^{rr,F} = \frac{2\pi k_r n_{max} R_{F,Diff}^6}{3R_0}, \tag{2.54}$$

$$D_D = \boldsymbol{M}^{rr,D} = \frac{k_{hop}}{6} n_{max} \lambda \left(3\lambda^4 + 6\lambda^3 R_0 + 6\lambda^2 R_0^2 + 4\lambda R_0^3 + 2R_0^4\right). \tag{2.55}$$

Note here that if we write the diffusion constant for Förster diffusion as $D_F = ck_r \frac{R_{F,Diff}^6}{a^4}$, we find $c = \frac{2\pi a}{3R_0} \approx 2.62$ as noted in Ref. [39], which is slightly below what was found in Refs. [31, 39]. This is not unexpected, since we are looking at a different lattice than the simple cubic lattice as used in those works. Throughout the rest of this chapter we have assumed uniform exciton density throughout space. The above derivation then does not make sense, since diffusion will have no effect on the exciton density directly. We can do this derivation for the two particle correlation function $g_2(r,t)$. As long as $\frac{r-2R_0}{R_{F,Diff}} \gg 1$ or $\frac{r-2R_0}{\lambda} \gg 1$ then the diffusion constants is simply the summation of the diffusion constants for the two particles related to the diffusion constants above. At lower distances the three site distribution affects the diffusion and causes advection away from the origin, due to less sites being available near the origin.

In order to derive this effect, we are going to assume the simplest form of nearest neighbour hopping $D(r) = k_{NN,hop}\delta(r - R_0)$. Using this definition in combination with $\boldsymbol{M}^i = n_{max} \int_V d\boldsymbol{\Delta}^3 D(\boldsymbol{\Delta}) \frac{\boldsymbol{\Delta}^i}{j!}$, where we use equation (2.14) in order to determine the integration volume, yields

$$\begin{aligned} \boldsymbol{M}_{g_2}^{r^i,NN} &= \frac{2\pi}{i!} R_0^{2+i} n_{surface} k_{NN,hop} \int_0^{\theta_{max}(r)} d\theta \sin(\theta) \cos^i(\theta) \\ &= \frac{2\pi R_0^{2+i} n_{surface} k_{NN,hop}}{(i+1)!} \left(1 - \cos^{1+i}(\theta_{max}(r))\right), \end{aligned} \tag{2.56}$$

where $\theta_{max}(r) = \mathrm{Re}\left(\pi - \tan^{-1}\left(\sqrt{\left[\frac{2R_0}{r}\right]^2 - 1}\right)\right)$. Note that also for Förster- and Dexter-type hopping advection will play a role at small distances, but then the strength of advection has to be determined numerically. Generally we will use as an approximation $\frac{4\pi R_0^4 n_{surface} k_{NN,hop}}{3}$ to be either $2D_D$ or $2D_F$. Note that here $\boldsymbol{M}_{g_2}^{r^i,NN}$ is now a function of distance r. In order to properly relate this to the Smoluchovski equation, we would need the generalised Smoluchovski equation, which will not be discussed here, but is discussed in more detail in Ref. [72].

Now that we know how our theory relates to the Smoluchovski equations and Fick's law of diffusion all there is left to do is to solve the Smoluchovski equation as shown in equation (1.7). We will be following Ref. [73] and looking at the TPQ process. We will be assuming that there is no potential between the triplet and polaron, thus we can set $U(r) = 0$. Furthermore as noted in Ref. [29] it is possible that merely Förster-type TPQ contributes significantly to the roll-off within Ph-OLEDs. In that case $S_R(r)$ is given by equation (2.36). In that case we can rewrite equation (1.7) as [73]

$$\frac{\partial g_{2,TP}(r,t)}{\partial t} = \frac{D_T + D_P}{r^2} \frac{\partial^2}{\partial^2 r} \left(r g_{2,TP}(r,t)\right) - k_r \left(\frac{R_{F,TPQ}}{r}\right)^6 g_{2,TP}(r,t). \tag{2.57}$$

Here again the boundary conditions as noted in equations (2.17) and (2.18) apply. These boundary conditions are not sufficient for solving this system. One needs an inner boundary at $r = R_0$. In Ref. [73] the no-diffusion boundary $\lim_{r \downarrow R_0} \frac{\partial g_{2,TP}(r,t)}{\partial r} = 0$ was proposed and the corresponding solution

$$\lim_{t\to\infty} g_{2,TP}(r,t) = \frac{2^{3/4}}{\Gamma(1/4)} z^{1/4}(r)\left[K_{1/4}(z(r)) + \frac{K_{3/4}(z(R_0))}{I_{-3/4}(z(R_0))} I_{1/4}(z(r))\right] \tag{2.58}$$

was found in equilibrium. Here $I_\alpha(x)$ and $K_\alpha(x)$ denote the modified Bessel functions and $z(r) = \frac{R_{F,TPQ}^3}{2r^2}\sqrt{\frac{k_r}{D_T+D_P}}$. We will compare our methods to this solution. Note that other inner boundary conditions have also previously been discussed in literature, such as in Refs. [74, 75].

3. Results and discussion

In this chapter we will discuss the results obtained using the theory as outlined in chapter 2. Part of this chapter can also be found in Ref. [37]. First we will discuss the results of the model in TRPL and steady state experiments without polarons nor diffusion in section 3.1. Then we will add the hopping of triplets in section 3.2. Thirdly we will look at the results including polarons and their hopping in section 3.3. Lastly we will compare the hopping diffusion to the Smoluchovski formalism. The results without polarons will be compared to KMC simulations. The KMC results were obtained by Mahyar Taherpour using Bumblebee [40].

3.1 Negligible triplet diffusion

In this section we will discuss the simplest situation in which there are neither polarons in the system nor are the triplets allowed to diffuse. This is also discussed in Ref. [37]. We will discuss both TRPL experiments and steady state operation of OLEDs.

3.1.1 Transient photoluminescent experiments

In TRPL experiments where the hopping of triplets is irrelevant, it has been verified before that the guest percentage of molecules is irrelevant [39] (assuming that guest molecules are not clumped together) and thus will not be taken into account. For example a system with 10% guest sites with 20% of sites initially containing an exciton will have the same response as a system with 100% guest sites at 2% initial occupation in this situation. We will focus on the comparison between different closures introduced in section 2.2 and the amount of initial excitons per Förster sphere ($\frac{4\pi n_0 R_{F,TTA}^3}{3}$) instead.

In figure 3.1 the exciton density as a function of time during a TRPL experiment is simulated for a phosphorescent OLED layer with $R_{F,TTA} = 3$ nm. Assuming that 100% of the emissive layer consists of phosphorescent material then here 2% of the sites initially contain an exciton, which are initially randomly spread throughout the material. For this situation we thus set $n_0 = 0.02$ nm^{-3}, such that the material initially contains 2.26 excitons per Förster sphere, where we have assumed $n_{max} = 1$ nm^{-3}. The time axis has been made dimensionless with regard to the radiative excitonic lifetime $1/k_r$. Here the KMC result can be assumed to be ground truth and is compared to the SPC closure (section 2.2.2), PA approximation (section 2.2.3) and the NCC first (mean-field) and second order (section 2.2.1).

From all results depicted in figure 3.1 it can be concluded that at low times the decay of excitons is non-exponential and faster than the exponential decay at large times. This indicates a significant contribution from TTA. At large times all curves except KMC decay with the same speed, indicating that the decay is purely due to radiative decay. The KMC results seem to curve upward slightly, although this is likely caused by insufficient statistics due to the low amount of particles in the system and we will disregard this. Both NCC first and second order fail quite dramatically with regards to the KMC results and start to deviate at $t \approx \frac{10^{-3}}{k_r}$ and $t \approx \frac{10^{-2}}{k_r}$ respectively. This indicates that the NCC closure is quite incorrect and we can only cutoff the system of equations at high order using this closure. This is not surprising, since the NCC closure assumes that the (higher order) covariance of excitonic occupation between sites in the system is negligible, which does not hold in this situation as we will conclude from figure 3.2. As can be noted both results using the SPC and PA closure are almost indistinguishable from the KMC result without the extra inset. We can thus note that both the PA and SPC are valid approximations in this scenario. In the case of limited computational resources and

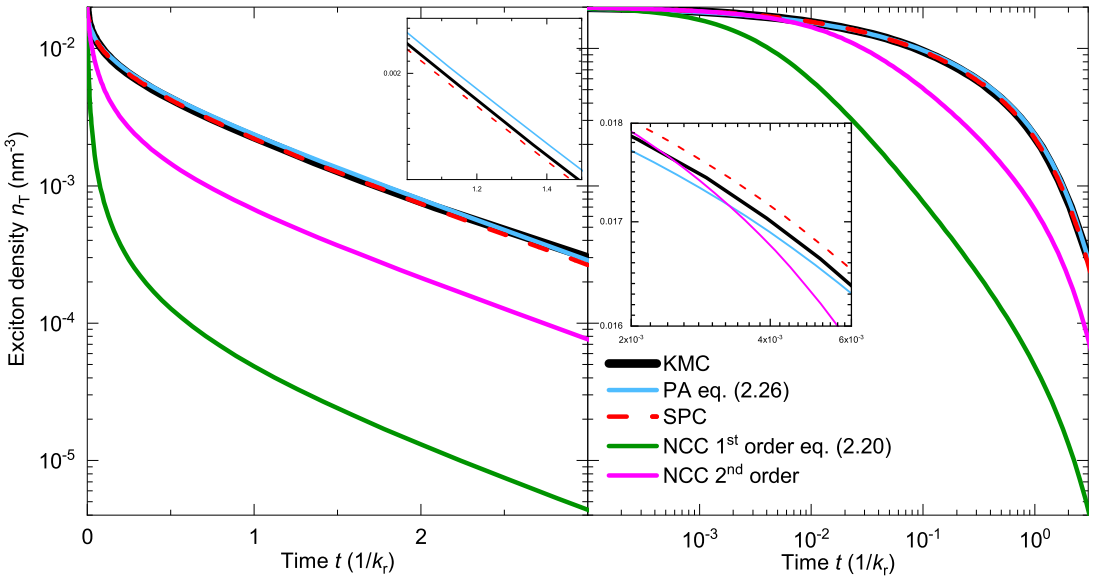

Figure 3.1: Density of triplets as a function of time $n_T(t)$ as simulated for during a TRPL experiment. The initial exciton density is set to $n_0 = 0.02$ nm^{-3}, diffusion of triplets is ignored and $R_{F,TTA} = 3$ nm. (a) Plot of transient densities where various different cutoffs applied to equations (2.9) and (2.10) as discussed in section 2.2 are denoted by the colored lines. These are compared to KMC simulations (thick solid black line). (b) Same plot using a logarithmic time axis. Insets indicate magnified areas.

time we recommend the PA result, while if extra accuracy is needed the SPC is recommended alongside KMC simulations. In the extra insets it can be seen that the the PA closure start underneath the KMC results and ends above the KMC results. For the SPC closure this is reversed, but the difference with the KMC results is smaller for SPC.

In figure 3.2 the pair correlation function $g_2(r,t)$ as a function of time for various distances of the closures described in section 2.2 are depicted and compared to the pair correlation found using KMC. These pair correlations are obtained during the simulations shown in figure 3.1 and do depend on the initial exciton density n_0. In the limit of $n_0 \to 0$ the SPC and PA results will become the same. First noticable result is the fact that NCC first order (mean-field) and second order are completely different than the KMC results. This due to the fact that the closure does not resemble the physical reality. This is partially caused by the fact that the closure is unphysical, since $g_2(r,t)$ dive below 2/3. The fact that the pair correlation function is overestimated by NCC results in overestimating the contribution of TTA, thus resulting in the reported exciton densities being too low as can be seen in figure 3.1. The PA results shows an acceptable agreement with the KMC results, but the pair correlation found using the PA drops early at larger distances in comparison to the KMC results. This explains the fact that the TTA effect is underestimated. The SPC closure has a near perfect agreement with the KMC results. This near perfect agreement raises questions as to why the results in figure 3.1 differ. This can only be explained by either the fact that different lattices were analysed or statistical fluctuations. It can be noted from the KMC, SPC and PA results that a correlation hole is created around every surviving exciton with radius $R_{corr} \propto R_{F,TTA}(k_r t)^{1/6}$ as noted in section 2.2.3.

In figure 3.3 the internal quantum efficiency as a function of the initial amount of excitons during a TRPL experiment is depicted as calculated using the PA and first order NCC (mean-field). The IQE is determined as $\int_0^\infty dt k_r \frac{n_T(t)}{n_0}$. Figure (a) shows the result for non-diffusing excitons as calculated in equation (2.26) using the PA closure, while figure (b) shows the case of strongly diffusing excitons as calculated in equation (2.20) as presented by the first order NCC closure. In both cases when there is one exciton per sphere with related characteristic radius the IQE has dropped to roughly 50%. For strongly diffusing excitons however this characteristic radius is

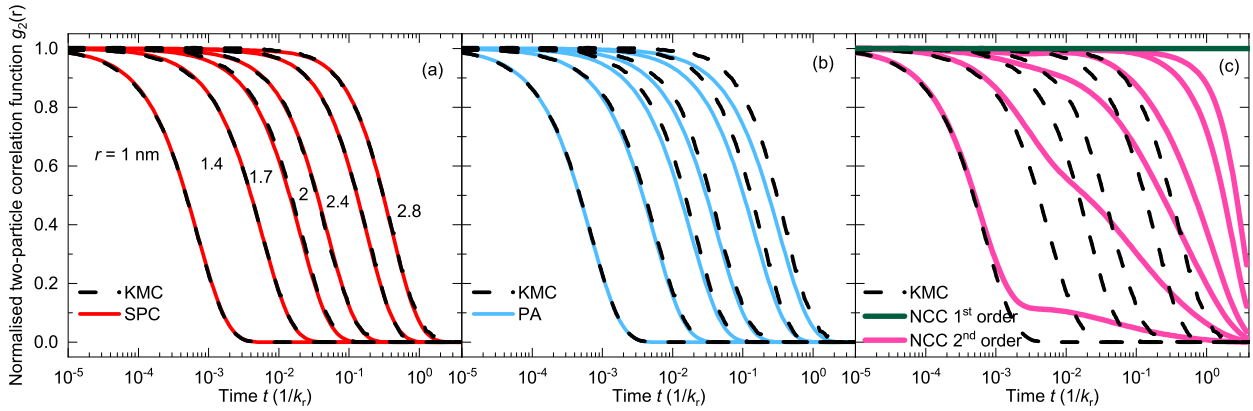

Figure 3.2: Triplet pair correlation function $g_{2,TT}(r,t)$ as a function of time t and distances r ($\in \{1, \sqrt{2}, \sqrt{3}, 2, \sqrt{6}, \sqrt{8}\}$ nm) during a TRPL simulation in the absence of the diffusion of triplets ($R_{F,Diff} = 0$) for $R_{F,TTA} = 3$ nm and initial exciton density $n_0 = 0.02$ nm^{-3}. The results for the SPC closure (a), PA closure (eq. (2.24)) (b), first and second order NCC (c) are compared to KMC results (black dashed lines).

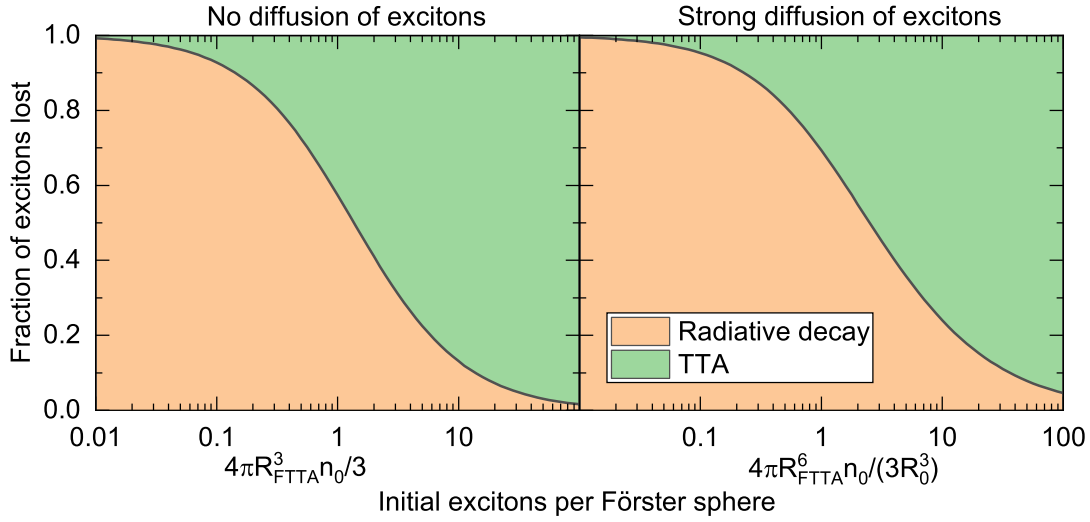

Figure 3.3: Portion of excitons lost due to either TTA or radiative decay ($\int_0^\infty dt k_r \frac{n_T(t)}{n_0}$) during a TRPL experiment as function of excitons per characteristic volume. (a) Excitons lost due to TTA in the no diffusion regime with $n_T(t)$ given by equation (2.26) as function of initial excitons per sphere with radius $R_{F,TTA}$. (b) Same as (a) in the strong diffusion regime with $n_T(t)$ given by equation (2.20). In (b) the solid black line plots $\frac{\ln(1+x)}{x}$, where $x = \frac{4\pi R^6_{F,TTA} n_0}{3R^3_0}$ or initial excitons per sphere with radius $\frac{R^2_{F,TTA}}{R_0}$.

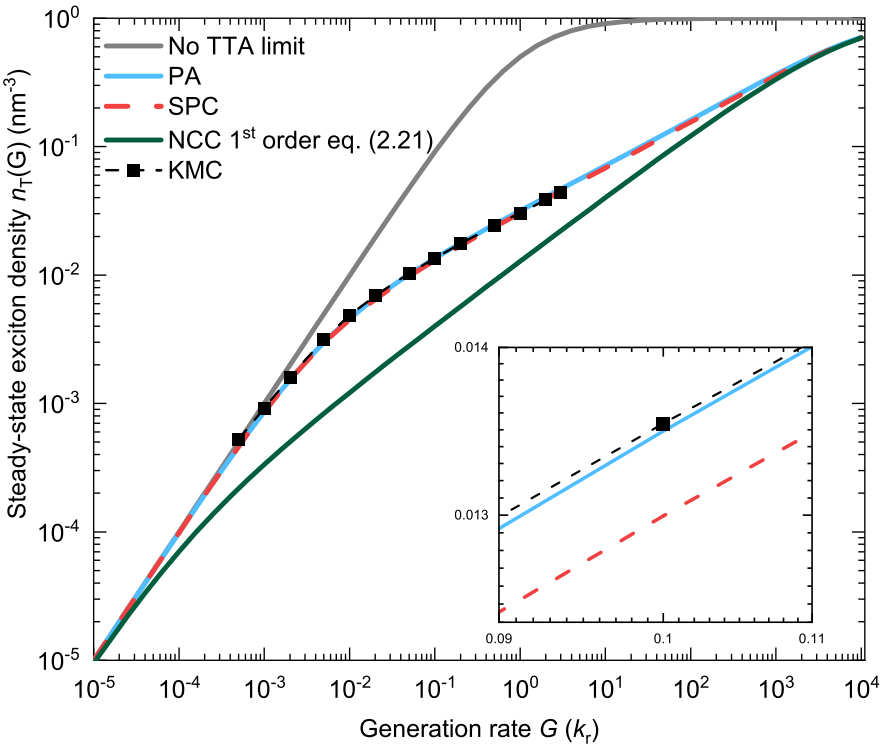

Figure 3.4: Density of triplet excitons $n_T(G)$ as a function of the generation rate G during steady-state operation for $R_{F,TTA} = 3$ nm in the absence of diffusion $R_{F,Diff} = 0$ nm. The different lines denote different closures applied to equation (2.10). The no-TTA limit is given by $n_T(G) = \frac{Gn_{max}}{k_r+G}$. Inset emphasises the difference between SPC, PA and KMC results.

generally much smaller than than for non-diffusing excitons. For non-diffusing excitons the characteristic radius equals the Förster radius $R_{F,TTA}$, while for strongly diffusing excitons this becomes $R_{F,TTA}\frac{R_{F,TTA}}{R_0}$. Due to the fact that generally $R^3_{F,TTA} \gg R^3_0$ we can conclude that strong diffusion greatly reduces the internal quantum efficiency at equal initial exciton density n_0.

3.1.2 Steady state operation

In steady state operation when diffusion is irrelevant, guest percentage of molecules does become relevant, but only changes the maximum amount of available sites n_{max}, by a factor c_{guest}. This does not drastically change the results and thus this variable will again be ignored.

During steady state operation a generation rate G is forced upon the system, where excitons are continuously generated and lost due to either TTA or radiative decay. We neglect electrons and holes in this section, thus this is most relevant for systems where the generation rate is caused by photon excitation, but can also represent recombination of electrons and holes in the bulk assuming a complete spatially uniform distribution of electrons and holes.

The exciton density $n_T(G)$ as a function of the generation rate is depicted in figure 3.4 for $R_{F,TTA} = 3$ nm. Again as before we note that the SPC and PA closures show excellent agreement with the KMC results, while the NCC result fails at quite low generation rates. The NCC results are correct for strongly diffusing excitons, which naturally causes the amount of excitons in the system to be lower. The three other results are equal to the no-TTA limit at low generation rates, due to there not being enough excitons in the system to react with. The

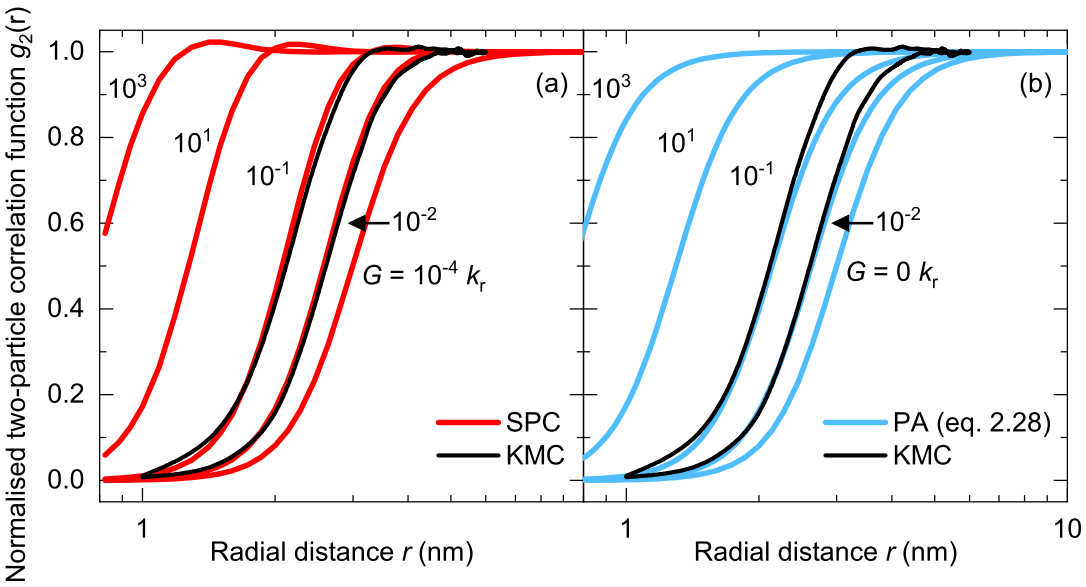

Figure 3.5: Exciton triplet pair correlation function $g_2\,(G, r)$ as a function of distance between a pair of exciton r for different generation rates G during steady state operation in the absence of diffusion ($R_{F,Diff} = 0$) for $R_{F,TTA} = 3$ nm. Here we compare the results obtained from KMC with the SPC closure (a) and PA closure (b).

no-TTA limit is given by taking the limit $R_{F,TTA} \to 0$ in equation (2.29), yielding $n_T\,(G) = \frac{Gn_{max}}{k_r+G}$. The border for the regime change as derived in equation (2.30) has become $G = 0.005\ k_r$, which agrees with the results shown in figure 3.4. In this intermediary regime TTA has become the dominant loss process. This causes the exciton density to grows as $n_T\,(G) \propto G^{1/3}$. At large generation rates we can see that the curve flattens around that region. Equation (2.30) predicts that this will happen at $G = 3.2 \cdot 10^4\ k_r$, which falls outside domain of the plot, but seems to nicely corresponds with the plotted data that shows flattening. In general actual OLEDs will not reach this regime and we have thus limited the x-axis. Furthermore in this regime other effects will start playing a role such as TPQ. The boundary between the intermediate and high generation regime should thus be taken with a grain of salt for actual OLED systems.

The inset in figure 3.4 emphasises the difference between KMC, PA and SPC results. We can conclude that the KMC results lie outside the range given by the PA and SPC results. It is closer to the PA result, even though the PA results should be less accurate. The KMC results are systematically higher than all other results, even than the no-TTA limit, which no results should be able to cross except due to statistical fluctuations. The deviation of the KMC results could be systematic errors related to the initial conditions. Here we possibly started with a initial exciton density unequal to the equilibrium value and did not simulate long enough.

In figure 3.5 the pair correlation function $g_2\,(G, r)$ is plotted as a function of distance between a pair of excitons for several values of the genenration rate and is compared between KMC and the SPC and PA closures. First thing to note is that all results seem to approximately adhere to the result of equation (2.28). At low distances, which most significantly contribute to TTA, all closures seem to yield equal results. This means that the corresponding exciton densities will be close to each other, which can be concluded from figure 3.4. Secondly SPC and KMC show an excellent agreement between each other, while the PA and KMC show a discrepancy between their tails. In order to derive the PA results we have ignored any three-particle correlations, which form the basis of this discrepancy. However still all results show a correlation hole being created with $R_{corr} \propto R_{F,TTA}\left(\frac{k_r n_T(G)}{G n_{max}}\right)$. It is interesting to note that while KMC and SPC show excellent agreement in figure 3.5 they do not in figure 3.4. This point tos either the lattice being very important in the steady state or there is a small systematic error in the KMC calculations, possibly due to initial conditions.

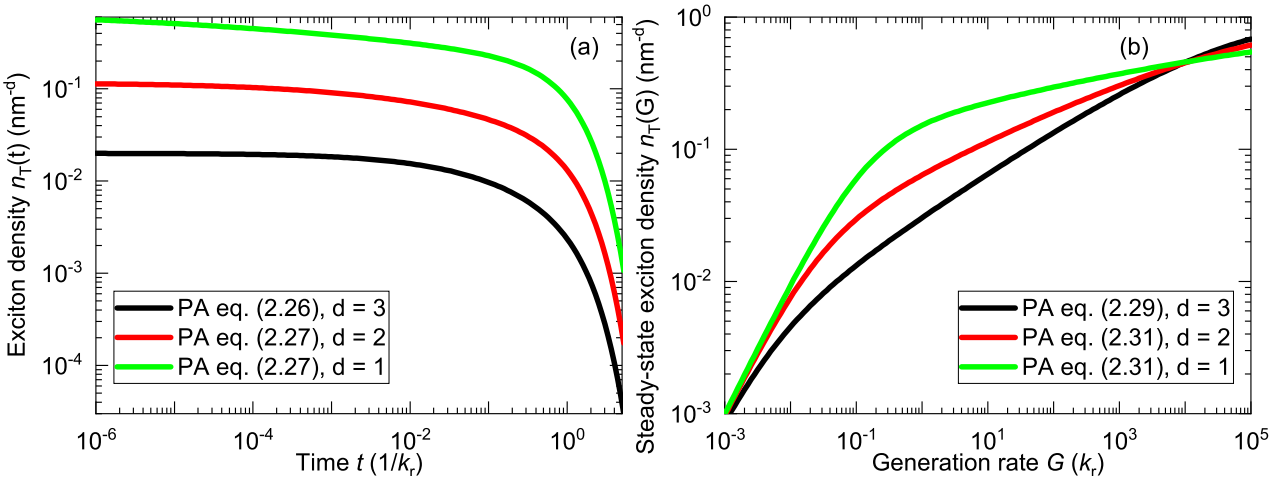

Figure 3.6: Density of triplets n_T for various spatial dimensionalities during a TRPL experiment (a) and in steady state (b) in the absence of diffusion for $R_{F,TTA} = 3$ nm using the PA closure. Note in this figure we have assumed $R_0 = 0$, which is incorrect at high exciton densities. For the TRPL experiment (a) the initial density is set such that $\frac{2^{\frac{d}{6}-1} n_0 \pi^{1+\frac{d}{2}} R_{F,TTA}^d}{3\Gamma\left(\frac{d}{2}\right)\sin\left(\frac{d\pi}{6}\right)}$ is constant and for $d = 3$ the initial exciton density equals $n_0 = 0.02$ nm^{-3}. In the steady state case (b) $n_{max} = 1$ nm^{-d}. Note that in this figure $R_0 = 0$ was assumed, which generally yields incorrect results at high exciton densities.

In the paragraphs above only the three dimensional case was analysed. However depending on the system the excitons might mainly be generated either on the surface with the electron or hole transport layer (ETL or HTL). Assuming the triplets do not hop, TTA happens approximately on a 2D plane. In that case we can use the PA results in any general dimensionality from equations (2.27) and (2.31) for the transient and steady state case respectively. The one, two and three spatial dimensional situations are plotted in figure 3.6. The fraction of initial sites occupied by excitons which is set constant is somewhat closely related to the IQE. More initial excitons are needed in order to lose the same fraction of excitons at lower dimensionalities. For the lower dimensionalities it can be seen that the exciton density decays as $t^{-d/6}$, while for the higher dimensionality this is less visible, due to the lower amount of excitons. In the steady state case at low generation rates the results are equal to the no TTA limit. Higher dimensionalities cause the intermediary regime to occur faster. However at lower dimensionalities the effect of TTA is more severe when it occurs, since $n_T(G) \propto G^{\frac{d}{6+d}}$.

3.2 Inclusion of triplet diffusion

In this section we will include the hopping of excitons throughout the material. There will be no polarons in the system, such that all space is available for exciton hopping as long as no other exciton are present. In literature it has been shown very frequently that diffusion mediates range-limited reactions. This has been shown for chemical reactions [76, 77], as well as for (Förster-like) donor-acceptor transfer [49, 78] as well as specifically for TTA [36, 39]. This summation of articles is far from complete or exhaustive. Now it is our turn to add results to this list of resources. We will first discuss TRPL experiments. Here we will come across the notion of percolation. Secondly we will also discuss steady state operation.

3.2.1 Transient photoluminscence experiments

In figure 3.7 we analyse the effect of diffusion and the percentage guest molecules, which are assumed to be the only sites excitons can jump towards, on the exciton density during a TRPL experiment. In figure 3.7 (a) we

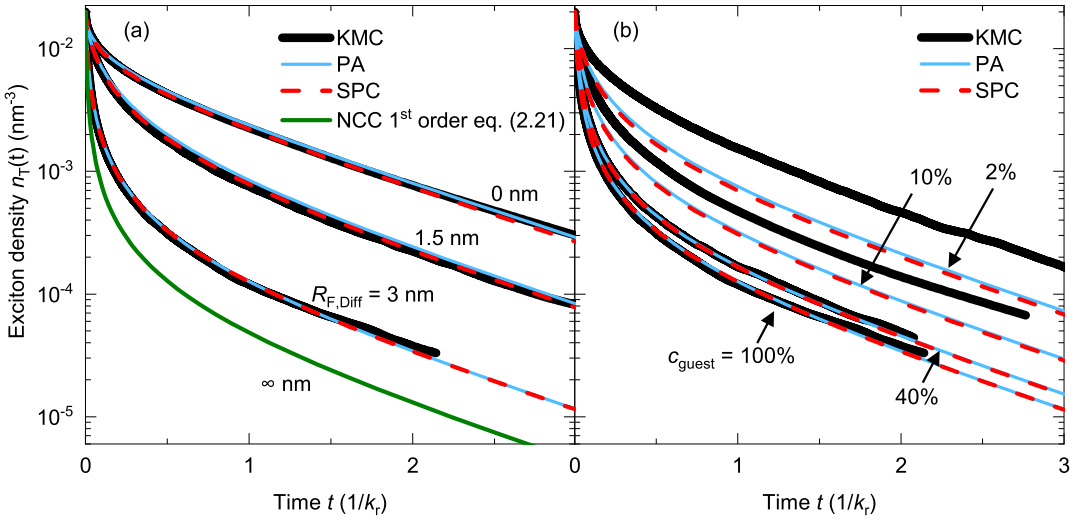

Figure 3.7: Exciton density $n_T(t)$ as a function of time with initial exciton density $n_0 = 0.02$ nm^{-3} and $R_{F,TTA} = 3$ nm for different diffusion strengths ($R_{F,Diff} \in \{0, 1.5, 3\}$ nm) at $c_{guest} = 100\%$ (a) and different percentages of guest molecules embedded within the host material ($c_{guest} \in \{2, 10, 40, 100\}\,\%$) at $R_{F,Diff} = 3$ nm (b). KMC results are compared to the SPC closure, PA closure and the infinitely strong diffusion limit denoted by the first order NCC closure.

can see the effect of diffusion. First of all as before both the PA and SPC results seem to be within statistical error and systematic error due the different lattice structure of the KMC results at $c_{guest} = 100\%$. Especially at large $R_{F,Diff}$ the SPC, PA seem to become the same. This is due to the fact that the exciton densities are much smaller and thus the approximation used for the PA results, becomes more accurate. Thus from the fact that when $R_{F,Diff}$ is set to larger values the exciton density decays faster and to lower value, means that the hopping rate increases the impact of TTA. The extra TTA that results from hopping steps before quenching will be called diffusion-mediated TTA. In the limit of $R_{F,Diff} \to \infty$ the mean field (NCC first order) results, here depicted in green, will be obtained for all simulation. Practically this will be realised when $R^6_{F,Diff} \gg R^6_{F,TTA}$. We also note that at large $R_{F,Diff}$ KMC will have both more statistical uncertainty due to the lower amount of excitons. The amount of events is increased with stronger diffusion, in turn increasing the computation time needed for KMC simulations, while it does not affect the computation time of our method.

In figure 3.7 (b) the results are shown for a naive implementation of lower c_{guest} than 100% for $R_{F,Diff} = 3$ nm $= R_{F,TTA}$. This naive implementation means that merely n_{max} is corrected by a factor c_{guest}. The site distribution function remains unchanged. In general at lower c_{guest} at any distance larger than some minimum radius of a molecule σ the site distribution function $\mu(r)$ will flatten to 1, but here we have already assumed that $\mu(r) = 1$ for $r > R_0$ and thus will not be adapted. Here $R_0 = \sigma$. As can be noted this works well until $c_{guest} = 40\%$, which is still above the site percolation threshold of nearest-neighbour interactions within a simple cubic lattice ($p_c \approx 0.307$ [79]). However as we can see at $c_{guest} = 10\%$ and 2% this naive implementation completely fails and seems to become worse with lower c_{guest}. As we went from calculating the proper system using (2.6) to the spatially averaged equation (2.7) local information of discrete sites was lost. In the KMC simulations there are actual discrete sites to which the excitons can jump retaining the local site distribution information. Due to the spatial averaging we are allowing excitons to jump to any site, but only a maximum amount of c_{guest} can exist on any site.

For any system where the hopping rate is proportional to $\frac{k_r R^\alpha_{hop}}{r^\alpha_{ij}}$ the time it takes to jump directly over a distance r_{ij} simply equals $\frac{r^\alpha_{ij}}{k_r R^\alpha_{hop}}$, while hopping over nearest neighbours the rate becomes $\frac{r_{ij} a^{\alpha-1}}{k_r R^\alpha_{hop}}$, where a denotes the nearest-neighbour distance. Since r_{ij} has to be larger than a, we find that for $\alpha > 1$ nearest neighbour hopping is preferred over direct hopping. This also holds for Förster-type transfer where $\alpha = 6$. Since our system always

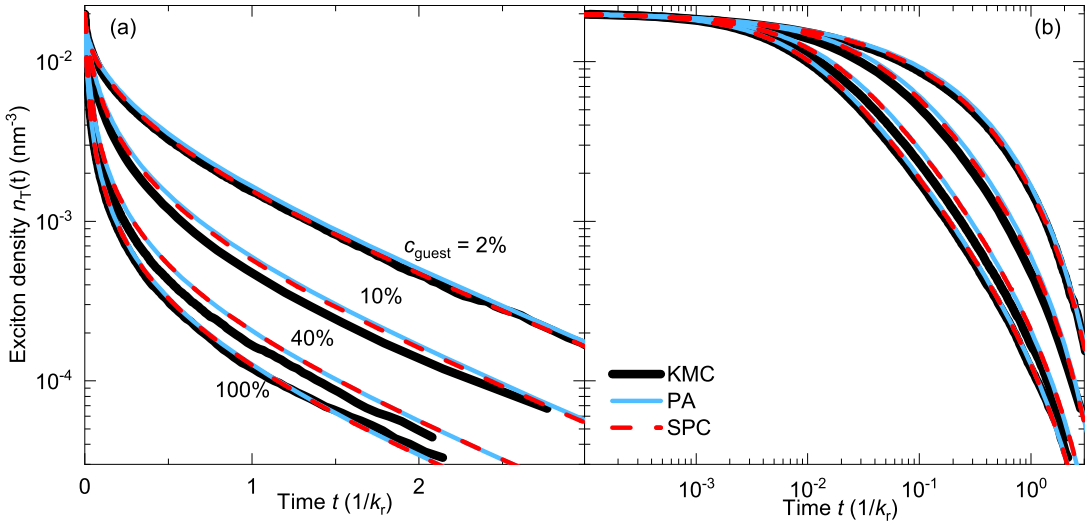

Figure 3.8: Exciton density $n_T(t)$ as a function of time with initial exciton density $n_0 = 0.02$ nm^{-3} and $R_{F,TTA} = 3$ nm and $R_{F,Diff} = 3$ nm with the effective lattice percolation model applied for different percentages of guest molecules ($c_{guest} \in \{2, 10, 40, 100\}$ %) within the host material. KMC results are compared to the SPC closure. The results are shown in linear timescale (a) and logarithmic timescale (b).

allows nearest-neighbour hopping, while KMC does not, we need to find a way to correct the average diffusion time from i to j in our method ($t_{i\to j} = \frac{1}{\sum_k 1/t_{i\to j,\text{route } k}}$). We propose an empirical method of dealing with this problem. Here we assume that the lattice is scaled for diffusion only. We propose the scaling

$$D(r) = \begin{cases} k_r \frac{R_{F,Diff}^6}{r^6} & r \geq R_0 c_{guest}^{-1/3} \\ 0 & \text{else} \end{cases}, \tag{3.1}$$

where the hopping rate itself has stayed equal, but the distribution of sites allowed to diffuse to only starts at $R_0 c_{guest}^{1/3}$. Plugging this into equation (2.54), yields that the diffusion coefficient D_F is proportional to $c_{guest}^{4/3}$, which was also concluded in Ref. [39]. This might explain why this method will work well. We will call this the effective lattice approach. This will not be completely correct, since percolation is very much dependent on the underlying lattice used in KMC. This will be most closely related to a lattice with the site distribution function as noted in chapter 2. For the rest of this thesis we will apply the effective lattice method when $c_{guest} < 100\%$. A very limited study of percolation for Förster-type diffusion can be found in the Appendix chapter B.

In figure 3.8 we now see the exciton density during a TRPL experiment, but for the SPC and PA results the effective lattice method outlined above was used. As can be noted these results are much closer for low c_{guest}, thus it seems that scaling a certain minimum distance by $c_{guest}^{-1/3}$ is correct in order to take into account percolation. Furthermore we can conclude that these results underestimate diffusion, since all results obtained using PA or SPC lie above the KMC results. Most likely the minimum cut-off distance of $R_0 c_{guest}^{-1/3}$ is too high or the lattice causes percolation effects. A possibility is to set this distance such that the size of one site stays equal to the inverse of n_{max}. This would yield a minimum distance of $a\left(\frac{3}{4\pi c_{guest}}\right)^{1/3}$, where a denotes the simple cubic lattice distance. This will not be explored here, since this methods are quite empirical.

In figure 3.9 we find the pair correlation functions $g_2(r,t)$ related to the exciton densities depicted in figure 3.7 (a) and 3.8. First thing to note when comparing to figure 3.2 is that the pair correlation function does not go to 0 for $t \to \infty$ for all distances r. This happens for the simple reason that the hopping of excitons allows, as given by outer boundary condition equation (2.18), decorrelation to creep in from infinitely far away. This is most noticable when diffusion is strongest as in figure 3.9 (b). This effect decreases when the strength of diffusion is

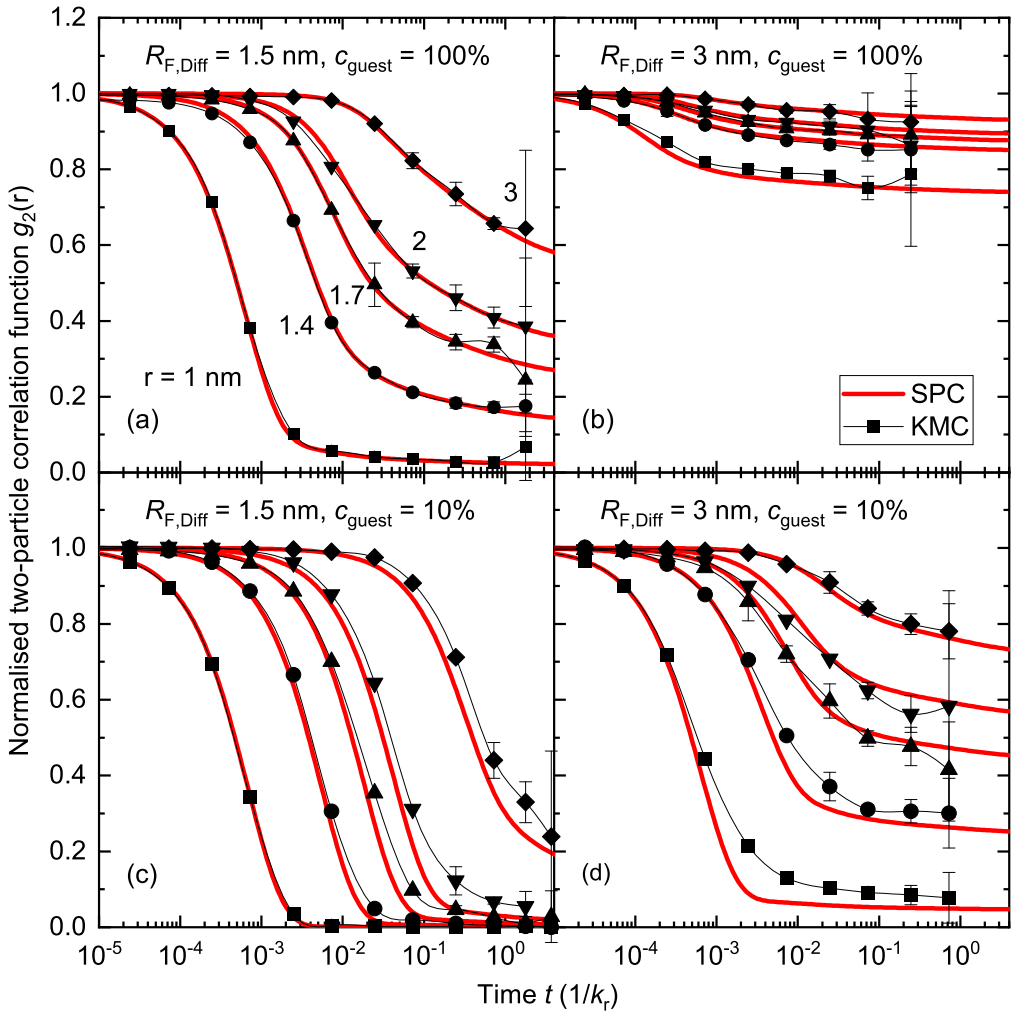

Figure 3.9: Pair correlation function $g_2(r,t)$ as a function of time for several relative distances between particles ($r \in \{1, \sqrt{2}, \sqrt{3}, 2, 3\}$) for $R_{F,TTA} = 3$ and diffusion radii $R_{F,Diff} = 1.5$ nm (a) and 3 nm (b). KMC results (black) are compared to the SPC closure results (red).

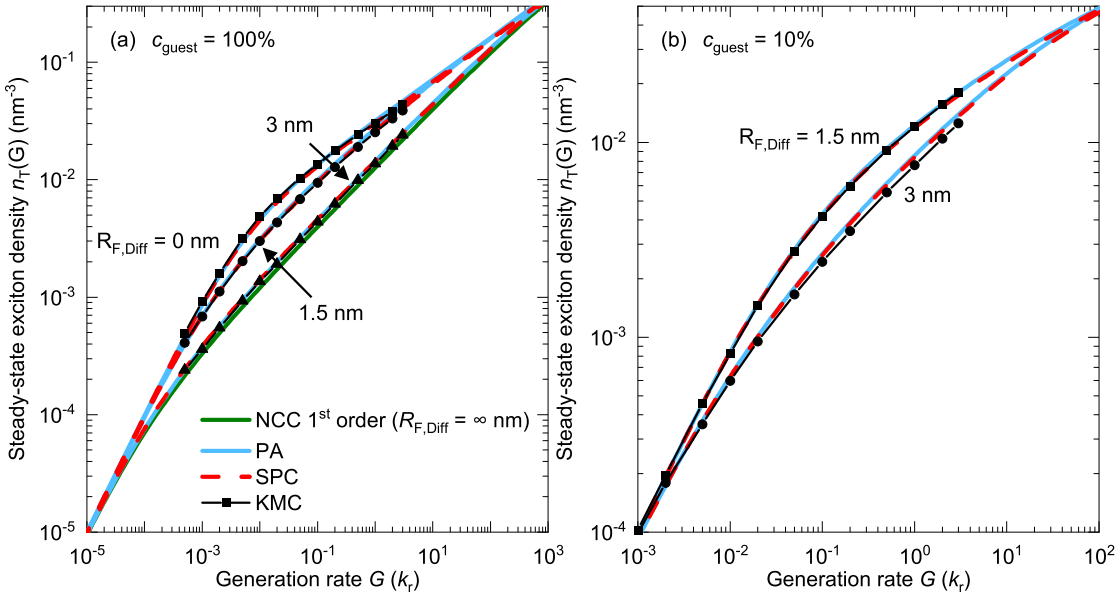

Figure 3.10: Triplet density $n_T(G)$ as a function of the generation rate G for $R_{F,TTA} = 3$ nm. Various values of the Förster diffusion radius $R_{F,Diff}$ are compared as well as the guest percentages 10% (b) and 100 % (a). KMC (black) results are compared to the SPC (red) and PA (blue) closures aswell as the strong diffusion limit first order NCC closure (green).

decreased, which happens when either $R_{F,diff}$ or c_{guest} is decreased. So the steady state value ($t \to \infty$) is larger for larger diffusion strengths and distances r, however as of yet we have not found an analytical solution for this. As can be seen for $c_{guest} = 100\%$ the SPC and KMC results show excellent agreement, which becomes merely acceptable at $c_{guest} = 10\%$. This is due to there not being any percolation effects at 100%, which do become significant at 10%. Our results seem to underestimate the pair correlation function, due to the underestimation of the diffusion strength, which corresponds to the exciton densities found in figure 3.10. Also note that at $R_{F,Diff} = 3$ nm, $c_{guest} = 100\%$ the decorrelation due to TTA is almost fully washed out, but not completely. For the $R_{F,Diff} = 1.5$ nm, $c_{guest} = 10\%$ the results at low distance resemble the no diffusion results in figure 3.2.

3.2.2 Steady state operation

In this subsection we will turn our heads to the steady state and analyse how the hopping of excitons influences the system. We will look at the dependence of the exciton density n_T and the pair correlation function g_2 on the Förster diffusion length $R_{F,Diff}$ and the guest percentage c_{guest}.

In figure 3.10 we depict the exciton density steady state for various values of $R_{F,Diff} \in \{0, 1.5, 3\}$ nm and $c_{guest} \in \{10\%\text{ (b)}, 100\%\text{ (a)}\}$. First of all again we note that both SPC and PA results are very close to the KMC results for all cases and thus can be used in order to do these simulations. At low generation rates all results are the same and equal to the no-TTA limit. At larger generation rates we notice for all results an intermediate regime. This intermediate regime does depend on the strength of diffusion. Higher values of $R_{F,Diff}$ cause the intermediate regime to occur earlier. In the intermediate regime the TTA contribution is dominant. The contribution of TTA is larger for large $R_{F,Diff}$, since the TTA is not merely single-step, but diffusion mediated multi-step TTA becomes prevalent. The hopping steps cause TTA to become more dominant. The intermediate regime boundary generation rate will always be in between $\frac{3k_r R_0^3}{4\pi n_{max} R_{F,TTA}^6} < G < k_r \left(\frac{2}{3}\pi^2 R_{F,TTA}^3 n_{max}\right)^{-1}$ which are the strong-diffusion and no-diffusion boundaries respectively. The exciton density in the intermediate regime is proportional to $G^{1/2}$ and $G^{1/3}$ for the the strong-diffusion and no-diffusion case respectively. The

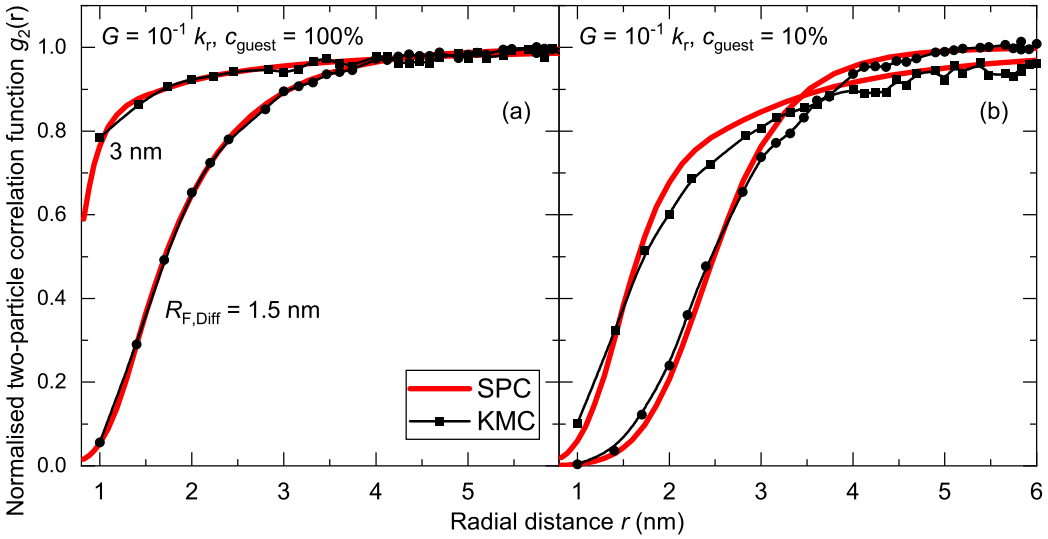

Figure 3.11: Pair correlation function $g_2(G,r)$ as a function of the distance for $G = 0.1\ k_r$, $R_{F,TTA} = 3$ nm for several values of $R_{F,Diff} \in \{1.5, 3\}$ nm in the case of $c_{guest} = 100\%$ (a) and $c_{guest} = 10\%$ (b). SPC results (red) are compared to KMC results (black).

$R_{F,Diff} = 1.5$ nm case in both plots seems to be proportional to $G^{1/2}$ at the lower generation rates in the intermediate regime and transform into $G^{1/3}$ at the higher intermediate generation rates. This is most likely caused by the fact that when the intermediate regime starts the excitons are still too far away from each other for single-step TTA, such that only multi-step TTA is dominant. In this case $R_{F,Diff}$ is low enough such that single-step TTA will become dominant at higher generation rates. It is interesting to note that $R_{F,Diff} = 3$ nm seems to practically already be the strong-diffusion limit in the case of $c_{guest} = 100\%$, which is lower than observed in the transient case. The results for $c_{guest} = 10\%$ seem to be approximately equal to the 100% results, except that n_T seems to be 10 times smaller and diffusion is slower. We do note that our results yield more excitons, due to the fact that our model does not perfectly account for percolation effects in the diffusion process. We underestimate diffusion as noted before and thus multi-step TTA is underestimated, causing the exciton density to be overestimated.

In figure 3.11 the pair correlation function is plotted in the case of $G = 0.1k_r$ for SPC and KMC results in figure 3.10. First thing to notice is that the SPC and KMC results show excellent agreement at $c_{guest} = 100\%$ for all $R_{F,Diff}$, while at $c_{guest} = 10\%$ SPC seems to slightly overestimate $g_2(G,r)$ relative to KMC. This however is in disagreement with the exciton density. Lower $g_2(G,r)$ means a lower contribution of TTA, thus should mean higher exciton densities in steady state. We however find the opposite in figure 3.10. This is quite remarkable, meaning that either there is a small calculation error in the KMC results, or the pair correlation function and the exciton density do not need to be correlated. Furthermore note the variability in the KMC results at large distances r. Since our method directly calculates averages, it thus has no statistical variability. This gives our method an advantage when calculating properties which need high amounts of statistics in order to converge during KMC simulations such as the pair correlation function $g_2(G,r)$. Furthermore we again note that higher $R_{F,Diff}$ and c_{guest} cause the steady state pair correlation to rise. This is due to the fact that decorrelation is allowed to diffuse inwards. This becomes stronger when these parameters are increased. The anti-correlation due to TTA is washed away. The correlation hole due to TTA is thus made smaller due to diffusion. Comparing figures 3.11 (a) and (b) it can be noted that at large distances in figure (b) the larger $R_{F,diff}$ causes $g_2(G,r)$ to dip down, while this does not happen in (a). The dipping down happens due to the anticorrelation being transported more efficiently towards the boundary condition (equation (2.18)), such that at low distances the pair correlations becomes higher and causing a bigger contribution from TTA, which in turn lowers the pair correlation at larger distances. In the case of $c_{guest} = 100\%$ the $R_{F,Diff}$ of 1.5 nm is too strong in order to see this effect. Furthermore particles can jump distances somewhat smaller than $R_{F,TTA}$, such that the change

from decorrelation, due to the boundary condition to the anti-correlation from TTA, can occur more rapidly. The results for PA are not shown here, since SPC and PA results are almost completely identical. The difference between PA and SPC in the tail of the correlation hole is washed out due to diffusion.

3.3 Inclusion of polarons

In this section we will evaluate the effect of polarons on the exciton density in TRPL experiments and steady state conditions. We will use the same parameters as shown in the sections above $R_{F,TTA} = 3$ nm, $n_0 = 0.02$ nm^{-3} and $R_0 \approx 0.79$ nm. We will assume that the excitons are confined to their initial position, thus $R_{F,Diff} = 0$ nm. Due to the fact that polarons generally hop over both guest and host sites. We will be assuming that the guest do not act as traps for the polarons. On top of these parameters we will be assuming $R_{F,TPQ} = 3.5$ nm, which is in line with values found in literature [70]. The polaronic density will be assumed to be $n_P = 10^{-3}$ nm^{-3}, which is inline with the polaronic density found in other simulations in literature [35, 80]. We will investigate the importance of the nearest neighbour hopping rate k_{hop} related to the localization length $\lambda = 0.6$ nm.

In figure 3.12 (a) the exciton density as a function of time for various values of k_{hop} is presented. First thing to note as always is that in limiting scenarios the no and strong diffusion limits found using the pair approximation are in agreement. There is a small difference in the no diffusion limit again due to the indirect single-step interaction not being taken into account properly for the PA results, while these are taken into account for the SPC results. Comparing the no diffusion result to figure 3.1, we note that the exciton density is slightly lower here. This is caused by TPQ, which concluding from figure 3.12 (b) is responsible to approximately 15% of the loss in the limit of $k_{hop} \to 0$. At larger values of k_{hop} we can conclude that the exponential decay rate at long simulation times ($t \to \infty$) becomes larger. This is caused by the fact that the decay rate at $t \to \infty$ has changed from k_r in the case without any polarons to $k_r + k_{TPQ,effective} n_P$. The steady state $k_{TPQ,t\to\infty}(k_{hop})$ is dependent on the strength of the hopping, but is between $0 \leq k_{TPQ,t\to\infty}(k_{hop}) \leq \frac{4\pi R^6_{F,TPQ}}{3R^3_0}$, where the boundaries are related to the limit of $k_{hop} \to 0$ and $k_{hop} \to \infty$ respectively. The TPQ rate coefficient k_{TPQ} increases with k_{hop}, due to TPQ moving from single-step TPQ to diffusion mediated multi-step TPQ. It seems that in this case $k_{hop} \gtrsim 7000\mu s^{-1}$ is the boundary transient hopping rate to the strong diffusion regime. We can also conclude this from figure 3.12 (b). From this figure we can furthermore conclude that the no diffusion regime seems to be below $k_{hop} \lesssim 1\mu s^{-1}$. We note that there are 2 regimes. The very weak and strong diffusion limits in which that TPQ rate is independent of the hopping rate (k_{hop}) and related diffusion coefficient, while in the intermediate regime the TPQ rate does depend on the hopping rate. This was also discussed in Refs. [73, 81].

In figure 3.13 (a) the exciton density in steady state $n_T(G)$ is plotted as a function of the generation rate for various values of k_{hop}. As is standard procedure by now, the limiting diffusion scenarios of the SPC simulations correspond to those derived by applying the pair approximation. Comparing this figure to figure 3.4 we conclude that at small generation rates the difference is small for non-diffusing polarons, while this deviation becomes larger for stronger diffusion. This is caused by the contribution of TPQ becoming stronger when polarons are allowed to diffuse and can thus quench more excitons. The TPQ rate coefficient is in between $\frac{2\pi^2}{3} k_r R^3_{F,TPQ} < k_{TPQ}(k_{hop}) < \frac{4\pi k_r R^6_{F,TPQ}}{3R^3_0}$. It is interesting to note that the intermediate regime is exactly the same as the non-diffusing case shown in figure 3.4 for all values of k_{hop}. This is caused by the fact that in this intermediary regime the TTA loss process is dominant. The intermediate regime is equal to the non-diffusing triplets scenario without polarons. This is confirmed by figure 3.13 (b), where $k_{hop} = 70\mu s^{-1}$. When result of $k_{hop} = 70\mu s^{-1}$ starts the intermediate regime at roughly $G = 10^{-2}\mu s^{-1}$ the TTA contribution quickly starts to take over the portion of excitons lost as shown in figure 3.13 (b).

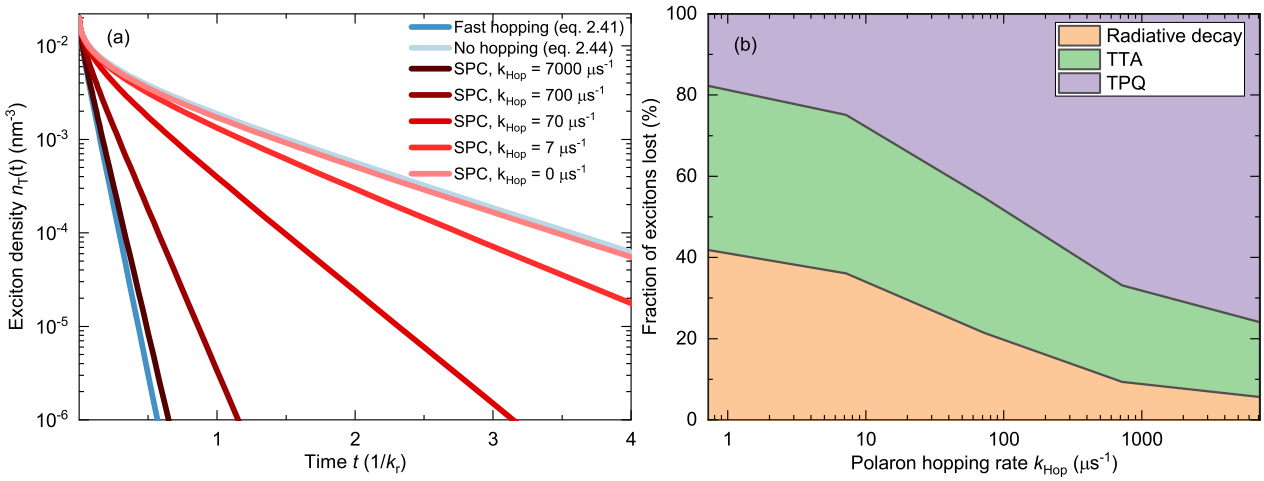

Figure 3.12: Exciton density as a function of time (a) and portion of excitons lost to different loss processes (b) during a TRPL experiment under the conditions of $R_{F,TTA} = 3$ nm, $n_0 = 0.02$ nm^{-3}, $R_{F,TPQ} = 3.5$ nm, polaronic localization length $\lambda = 0.6$ nm and polaron density $n_P = 0.001$ nm^{-3} for different values of the nearest-neighbour hopping rate k_{hop}. The two limits of no-diffusion and strong diffusion are plotted in blue (a), but for diffusion in between the results are in red where SPC was used. In figure (b) the orange area indicates the IQE at different values of k_{hop}.

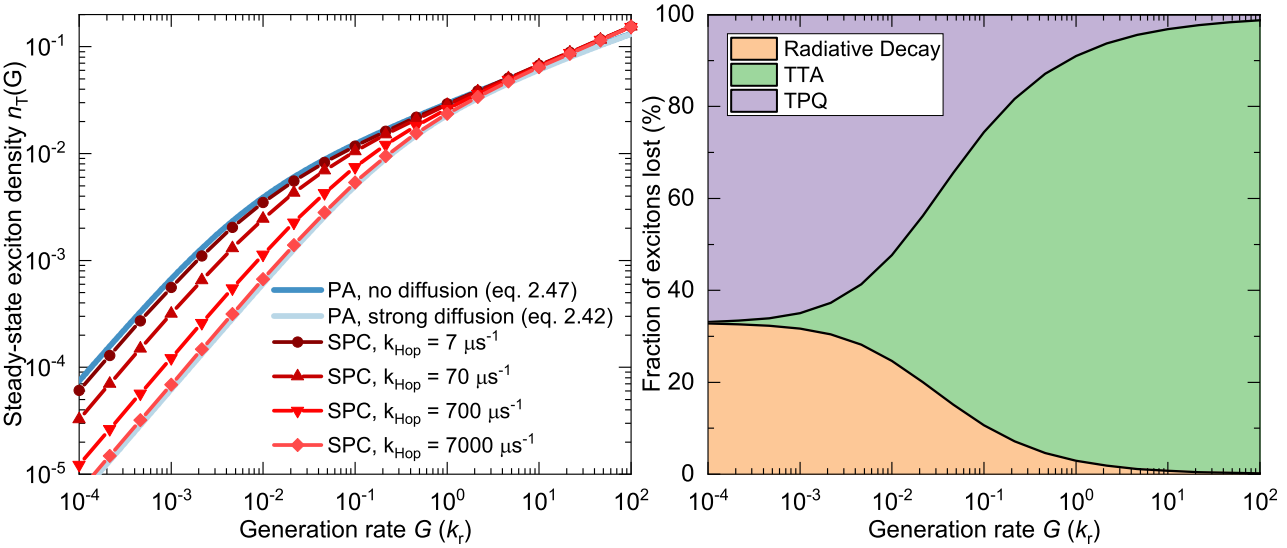

Figure 3.13: In (a) the steady state exciton density is plotted as a function of the generation rate under the conditions of $R_{F,TTA} = 3$ nm, $R_{F,TPQ} = 3.5$ nm, polaronic localization length $\lambda = 0.6$ nm and polaron density $n_P = 0.001$ nm^{-3} for different values of the nearest-neighbour hopping rate k_{hop}. In (b) the portions of excitons lost to different loss processes as a function of the generation rate G under the same conditions as (a) plus $k_{hop} = 70\mu$s^{-1}.

3.4 Comparison to Smoluchovski equation

Up until this point we have only compared our technique to mean-field modelling and KMC simulations. In this section we will compare our method with the Smoluchovski equations.

We will follow Ref. [73] and look at a system with TPQ, but without TTA. In that case the time evolution of the triplet-polaron correlation function can be approximated using equation (2.57) as predicted using Smoluchovski theory. Our theory predicts diffusion differently as given in equation (2.39). We use these to simulate a TRPL experiment until steady state $t \to \infty$. The steady state result is shown in figure 3.14. Here we used the parameters $R_0 = 1$ nm, $R_{F,TPQ} = 3$ nm and $\lambda = 0.6$ nm. We can conclude that at intermediate distance the results are quite alike for the diffusion coefficients related to the paremeters in our own theory as predicted by equation (2.55). At both the lower and higher distances this does not seem to be the case. At low distances the boundary condition seems to be the main cause of deviation. We have assumed for the Smoluchovski formalism $\lim_{r \downarrow R_0} \frac{\partial g_{2,TP}(r,t)}{\partial r} = 0$. Our own theory does not need a boundary condition at the inner boundary aside from the site distribution functions. It however seems that our theory predicts that $\lim_{r \downarrow R_0} \frac{\partial g_{2,TP}(r,t)}{\partial r} = \frac{C}{r^2}$, where C is some constant, indicating that only the diffusion term in the Smoluchovski equation (2.57) needs to be 0 at the boundary, since particles will not be able to diffuse here. We were however not able to find a relation for the parameter C as a function of k_{hop}. At large distances we once more see a deviation. Our theory seems to have less contribution due to diffusion than the Smoluchovski theory. This could be due to the fact that the Smoluchovski theory allows particle to move infinitesimally small distances, which we do not allow. We thus note that our theory can be approximated by Smoluchovski theory, but will yield different results. This might indicate that the Smoluchovski theory needs a different inner boundary condition. The results might be somewhere in between both results for actual materials, since the site distribution function we assumed might

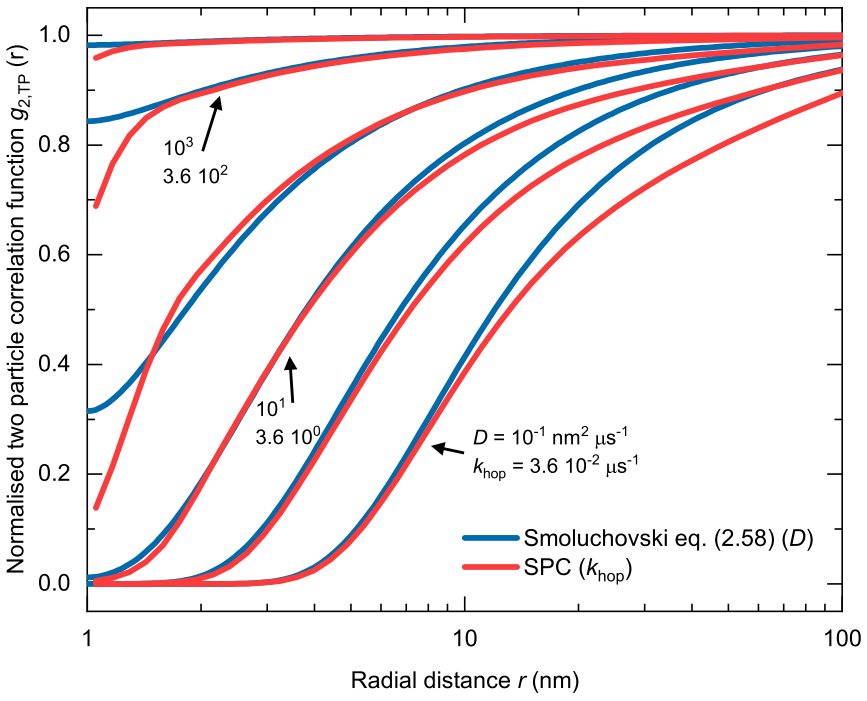

Figure 3.14: Triplet-polaron correlation function as a function of relative distance r in steady state after a TRPL experiment ($t \to \infty$) for various diffusion strengths D and k_{hop} for the parameters $R_{F,TPQ} = 3$ nm, $\lambda = 0.6$ nm and $R_0 = 1$ nm. We compare the Smoluchovski equations (blue) with our own modelling presented in chapter 2 (red).

not equal to reality.

4. Conclusion and outlook

In this thesis in chapter 2 we have developed a model that takes into account the spatial decorrelation due to bimolecular loss processes, here specifically triplet-triplet annihilation and triplet-polaron quenching, which is often ignored in literature. Our methods were inspired by recent work on charge transport presented in Ref. [44]. We started from the classical master equation where all relevant physical processes were included and by determining statistical averages and correlations we ended up with a BBGKY hierarchy of equations. We then translated this into a continuum model, where the distribution of sites throughout the material remained general as long as it was uniform throughout the material. We discussed several closures in order to close the BBGKY hierarchy of equations and allowing us to solve coupled differential equations. We specifically introduced the Kirkwood superposition closure (SPC), stemming from Ref. [53], the negligible correlation closure (NCC), based on Ref. [44] and our own pair approximation closure (PA) based on taking the limit of low exciton density. This last closure allowed us to create new analytical expressions of the exciton density for perfectly confined excitons. Lastly we shortly compared our method involving our integral representation of hopping in continuum to the more generally used Smoluchovski formalism based on derivatives [50] and derived a relation between the diffusion constant and the Förster radii related to diffusion.

In chapter 3 the actual results of our model were presented. By comparing our results of the exciton density in a system with merely single-step TTA with KMC results, we were able to judge the accuracy of the different closures. We concluded that the SPC closure gave the most accurate results, while being computationally the most expensive. Our developed pair approximation method gave results which were on par in terms of accuracy with the KMC and SPC results, while being computationally much cheaper and even allowing for analytical results in limiting scenarios. The NCC closure [44] proved to be less successful in the case that triplets are confined, only becoming correct in the limit of strongly diffusing triplets. We furthermore were able to derive the start of the roll-off curve due to TTA with and without diffusion of triplets for TRPL experiments and during steady state operation. We quantified the deviation from the exponential radiative decay due to TTA. During the steady state operation we found that in the roll-off the exciton density should grow with the generation rate as $G^{1/3}$ or $G^{1/2}$ for non-diffusing and strongly diffusing excitons respectively, where the generation rate should be linked to the current density through either the SRH model or Langevin recombination model or more advanced modelling techniques. Our method furthermore gives computationally cheaply insight into the two- (and three-particle) correlation functions and we have derived the size of the correlation hole created around every exciton due to TTA and TPQ. We furthermore derived that this correlation hole becomes smaller with increased generation rate and increased diffusion strength as would be expected. We did run into percolation issues when looking at diffusion in host-guest systems. We used an empirical method based on the scaling of the diffusion coefficient in order to account for these percolation issues. Lastly we concluded that the hopping rate of polarons has a detrimental effect on the amount of excitons in the system. We quantified this effect of the mediation of diffusion within TPQ on the exciton density.

4.1 Outlook

As noted in chapter 3 we have introduced an effective lattice method in order to take into account percolation effects. This effective lattice method was an empirical method based on what we saw during KMC simulations. This method however seems to underestimate the diffusion. It has been noted before that the diffusion coefficient should go as $c_{guest}^{4/3}$ [39], however this might not hold at guest percentages near 100% nor at short time scales. This could be caused by the difference between a discrete (simple cubic) lattice and the continuum description, nevertheless it would be interesting to further explore this. This would mean an indepth study of percolation theory on site percolation on discrete lattices with long-range interactions. It would be interesting to investigate

the actual lattices within OLED structures and the effect a specific lattice has on the diffusion strength.

In this work we have completely ignored the energy disorder of triplets. This assumption is generally incorrect and can have a large influence on the diffusion rates[82, 83]. We did try to assume a density of states with a Gaussian disorder, while assuming that the excitons occupied density of states behaves as a Fermi-Dirac distribution. This however yields inaccurate results. Since energy disorder is quite important for the diffusion of excitons, one could try to find a way to incorporate energy disorder into this model. This might again mean that percolation effects have to be taken into account. It might be interesting to look at the theory used within the correction energy concept from Ref. [84].

Throughout this thesis we have only focused on modelling second generation OLEDs. In these OLED stacks intersystem crossing is sufficiently fast such that we can assume all excitons are triplets [17, 18]. This does not hold however for TADF-OLED systems, where excitons repeatedly convert from triplet to singlet and vice versa. The notions of spatial correlations however can also be important for these kinds of systems. This is amplified, since not only is the continuous conversion important, but also singlet-singlet and singlet-triplet annihilation can become significant or even dominant [85]. It would be interesting to bring the principle of master equation modelling with the focus on spatial correlation to TADF OLEDs.

Lastly in this work we have assumed that excitons are generated uniformly throughout the material with some generation rate G. This is a proper assumption when the generation of excitons occurs by excitation from photons. In commercial products this only tends to happen by recombination of electrons and holes. Two of the most succesful, but simple model for calculating the recombination rate of electrons and holes are the Langevin and Shockley-Read-Hall recombination models [86, 87]. It might be interesting to apply the technique outlined in chapter 2 to a system with electrons and holes including coulomb interactions in order to improve upon these models. Furthermore electrons and holes generally are not uniformly spread out over the system. It would be interesting to apply the technique outlined in chapter 2, but without the averaging over space as done in equation (2.7). This will require extra computer resources, but allows for taking into consideration percolation effects. Such a study was already performed in Ref. [44], but recombination, excitons, PA and/or the SPC closure could be added to these calculations.

5. Acknowledgements

Even though the entirety of the my Master thesis period was spent during the coronavirus pandemic, it did not feel like bizarre thanks to the lovely people at the Molecular Materials and Nanosystems (M2N) group. I had lots of lovely discussions with people, albeit it mostly online and am thankful for all. I do need to mention several people in particular.

First of all I want to express my gratitude to my direct supervisor prof. dr. Peter Bobbert. Thank you first of all for teaching me the basics of organic electronics. I really appreciated the time you invested for my everlasting questions, while also asking critical questions in return. I think I speak for my parents and girlfriend aswell when I say that I admire your patience with my questions and occasional chaoticity, but am forever grateful. All of this made me overenthusiastic about our project and OLEDs in general and caused me to want to do much more than we had initially envisioned. Luckily you made sure that we finished a project and stayed on the right track instead of flying off into all directions. All of this resulted into a very paper that is going to be published and my master thesis of which I am very proud thanks to you.

That brings me to my second supervisor MSc. Mahyar Taherpour. I am very grateful for you taking me in on your MEMOLED project. I will fondly remember cursing at Python and Origin on Fridays trying to compare our results to KMC results you graciously made and how you just simply solved my 'huge' programming problem in a matter of minutes over the mail. I really appreciated our passionate discussions which definitely ended up improving my work and thinking and hopefully yours aswell. When I was being overenthusiastic about everything you helped me realise that doing proper literature research can be more fruitful. I was impressed with the papers you were able to dig up from decades ago, but very relevant and helpful to our research and making us think. Lastly I am really thankful I got to tag along with your first paper and am looking forward to your future works!

I should definitely also mention prof. dr. Reinder Coehoorn. Your everlasting ideas have at times really propelled us forwards. Your ideas immensely helped us to develop the PA closure. I really enjoyed your everlasting enthusiasm for all physics at any time especially during the OLED brainstorms. I furthermore very much appreciated your critical questions during the OLED brainstorms and am very much looking forward to my next adventure in Karlsruhe which you helped organise!

Obviously I would never forget the ever helpful and talkative Margot Gordon-Buteijn. I appreciated that you helped me get settled in the group during this bizarre period. I had a lot of fun during the weekly online coffee meetings, even when in the end we were practically the only ones left! Lastly I will be forever grateful your listening ear and organising capabilities.

I also need to mention the OLED group, consisting of Christoph, Lois, Christ, Stan, Stefano, Harm, Engin and Eline for the ever engaging discussions on Wednesdays. Although the entirety of the M2N group was amazing. Lastly thank you and I apologise to all my friends and family for having to bear my everlasting lectures on OLEDs for (apparently not so) laymen.

If you made it this far then I also want to thank you, the reader, for reading this work.

Bibliography

[1] Brijesh Kumar, Brajesh Kumar Kaushik and Yuvraj Singh Negi. "Organic thin film transistors: structures, models, materials, fabrication, and applications: a review". In: *Polymer Reviews* 54.1 (2014), pp. 33–111.

[2] Omar A. Abdulrazzaq et al. "Organic solar cells: A review of materials, limitations, and possibilities for improvement". In: *Particulate Science and Technology* 31.5 (2013), pp. 427–442. ISSN: 02726351. DOI: 10.1080/02726351.2013.769470.

[3] Gloria Hong et al. "A Brief History of OLEDs—Emitter Development and Industry Milestones". In: *Advanced Materials* 33.9 (2021), p. 2005630. ISSN: 15214095. DOI: 10.1002/adma.202005630.

[4] Nobel Foundation. *The Nobel Prize in Chemistry*. 2000. URL: https://www.nobelprize.org/prizes/chemistry/2000/press-release/.

[5] Seth C. Rasmussen. "Early history of conductive organic polymers". In: *Conductive Polymers*. CRC Press, 2018, pp. 1–22. DOI: 10.1201/9781315119007-1.

[6] J Stark and W Steubing. "Fluoreszenz und lichtelektrische Empfindlichkeit organischer Substanzen". In: *Physik. Zeitschr* 15 (1908), pp. 481–495.

[7] C. W. Tang and S. A. Vanslyke. "Organic electroluminescent diodes". In: *Applied Physics Letters* 51.12 (1987), pp. 913–915. ISSN: 00036951. DOI: 10.1063/1.98799.

[8] Ranbir Singh et al. "Improving the contrast ratio of OLED displays: An analysis of various techniques". In: *Optical Materials* 34.4 (2012), pp. 716–723. ISSN: 09253467. DOI: 10.1016/j.optmat.2011.10.005.

[9] Aditi Khazanchi et al. "OLED: A New Display Technology". In: *International Jouranal of Engineering And Computer Science* 1.2 (2012), pp. 75–84.

[10] P. E. Burrows et al. "Reliability and degradation of organic light emitting devices". In: *Applied Physics Letters* 65.23 (1994), pp. 2922–2924. ISSN: 00036951. DOI: 10.1063/1.112532.

[11] David J Griffiths and Darrell F Schroeter. *Introduction to quantum mechanics*. Cambridge University Press, 2018. ISBN: 978-0131118928.

[12] Emilia Arisil et al. "Spin polarized electrodes for organic light emitting diodes". In: *2004 4th IEEE Conference on Nanotechnology* 5.6 (2004), pp. 140–142. DOI: 10.1109/nano.2004.1392276.

[13] W. Helfrich and W. G. Schneider. "Transients of volume-controlled current and of recombination radiation in anthracene". In: *The Journal of Chemical Physics* 44.8 (1966), pp. 2902–2909. ISSN: 00219606. DOI: 10.1063/1.1727152.

[14] Xander de Vries. "Charge and exciton transport in organic semiconductors: the role of molecular vibrations". English. Proefschrift. PhD thesis. Technische Universiteit Eindhoven, Sept. 2019. ISBN: 978-90-386-4851-4.

[15] Chihaya Adachi et al. "High-efficiency organic electrophosphorescent devices with tris(2-phenylpyridine)iridium doped into electron-transporting materials". In: *Applied Physics Letters* 77.6 (2000), pp. 904–906. ISSN: 00036951. DOI: 10.1063/1.1306639.

[16] M. A. Baldo, C. Adachi and S. R. Forrest. "Transient analysis of organic electrophosphorescence. II. Transient analysis of triplet-triplet annihilation". In: *Physical Review B - Condensed Matter and Materials Physics* 62.16 (2000), pp. 10967–10977. ISSN: 01631829. DOI: 10.1103/PhysRevB.62.10967.

[17] Martin Kleinschmidt, Christoph Van Wüllen and Christel M. Marian. "Intersystem-crossing and phosphorescence rates in fac-IrIII(ppy)3: A theoretical study involving multi-reference configuration interaction wavefunctions". In: *Journal of Chemical Physics* 142.9 (2015), p. 94301. ISSN: 00219606. DOI: 10.1063/1.4913513.

[18] Gordon J. Hedley, Arvydas Ruseckas and Ifor D.W. Samuel. "Ultrafast luminescence in Ir(ppy)3". In: *Chemical Physics Letters* 450.4-6 (2008), pp. 292–296. ISSN: 00092614. DOI: 10.1016/j.cplett.2007.11.028.

[19] A. Köhler and H. Bässler. "Triplet states in organic semiconductors". In: *Materials Science and Engineering R: Reports* 66.4-6 (2009), pp. 71–109. ISSN: 0927796X. DOI: 10.1016/j.mser.2009.09.001.

[20] Hiroki Uoyama et al. "Highly efficient organic light-emitting diodes from delayed fluorescence". In: *Nature* 492.7428 (2012), pp. 234–238. ISSN: 00280836. DOI: 10.1038/nature11687.

[21] Hajime Nakanotani et al. "High-efficiency organic light-emitting diodes with fluorescent emitters". In: *Nature Communications* 5.1 (2014), pp. 1–7. ISSN: 20411723. DOI: 10.1038/ncomms5016.

[22] Hartmut Yersin et al. "Design of a New Mechanism beyond Thermally Activated Delayed Fluorescence toward Fourth Generation Organic Light Emitting Diodes". In: *Chemistry of Materials* 31.16 (2019), pp. 6110–6116. ISSN: 15205002. DOI: 10.1021/acs.chemmater.9b01168.

[23] Robert Pollice et al. "Organic molecules with inverted gaps between first excited singlet and triplet states and appreciable fluorescence rates". In: *Matter* 4.5 (2021), pp. 1654–1682. ISSN: 25902385. DOI: 10.1016/j.matt.2021.02.017.

[24] Sebastian Reineke, Karsten Walzer and Karl Leo. "Triplet-exciton quenching in organic phosphorescent light-emitting diodes with Ir-based emitters". In: *Physical Review B - Condensed Matter and Materials Physics* 75.12 (2007), p. 125328. ISSN: 10980121. DOI: 10.1103/PhysRevB.75.125328.

[25] Xander De Vries et al. "Triplet exciton diffusion in metalorganic phosphorescent host-guest systems from first principles". In: *Physical Review B* 99.20 (2019), p. 205201. ISSN: 24699969. DOI: 10.1103/PhysRevB.99.205201.

[26] Anna Köhler and Heinz Bässler. *Electronic processes in organic semiconductors: An introduction.* John Wiley & Sons, 2015, pp. 1–405. ISBN: 9783527685172. DOI: 10.1002/9783527685172.

[27] Caroline Murawski, Karl Leo and Malte C. Gather. "Efficiency roll-off in organic light-emitting diodes". In: *Advanced Materials* 25.47 (2013), pp. 6801–6827. ISSN: 09359648. DOI: 10.1002/adma.201301603.

[28] Michael Kasha. "Characterization of electronic transitions in complex molecules". In: *Discussions of the Faraday Society* 9 (1950), pp. 14–19. ISSN: 03669033. DOI: 10.1039/DF9500900014.

[29] H. Van Eersel et al. "Monte Carlo study of efficiency roll-off of phosphorescent organic light-emitting diodes: Evidence for dominant role of triplet-polaron quenching". In: *Applied Physics Letters* 105.14 (2014), 156_1. ISSN: 00036951. DOI: 10.1063/1.4897534.

[30] Sebastian Wehrmeister et al. "Combined electrical and optical analysis of the efficiency roll-off in phosphorescent organic light-emitting diodes". In: *Physical Review Applied* 3.2 (2015), p. 24008. ISSN: 23317019. DOI: 10.1103/PhysRevApplied.3.024008.

[31] Th Förster. "Intermolecular energy transfer and fluorescence." In: *Ann. Phys. Leipzig.* 2 (1948), pp. 55–75.

[32] D. L. Dexter. "A theory of sensitized luminescence in solids". In: *The Journal of Chemical Physics* 21.5 (1953), pp. 836–850. ISSN: 00219606. DOI: 10.1063/1.1699044.

[33] Franz Symalla et al. "Multiscale Simulation of Photoluminescence Quenching in Phosphorescent OLED Materials". In: *Advanced Theory and Simulations* 3.4 (2020), p. 1900222. ISSN: 25130390. DOI: 10.1002/adts.201900222.

[34] Harm van Eersel. "Device physics of organic light-emitting diodes: interplay between charges and excitons". PhD thesis. Technische Universiteit Eindhoven, 2015. ISBN: 978-90-386-3949-9.

[35] Jeroen Cottar. "Modeling of charge-transport processes for predictive simulation of OLEDs". PhD thesis. Technische Universiteit Eindhoven, 2012. DOI: 10.6100/IR740068.

[36] H. Van Eersel, P. A. Bobbert and R. Coehoorn. "Kinetic Monte Carlo study of triplet-triplet annihilation in organic phosphorescent emitters". In: *Journal of Applied Physics* 117.11 (2015), p. 115502. ISSN: 10897550. DOI: 10.1063/1.4914460.

[37] Mahyar Taherpour et al. "Accurate and fast master equation modeling of triplet-triplet annihilation in organic phosphorescent emission layers including correlations". In: *Phys. Rev. B* (in press).

[38] Reinder Coehoorn et al. "Kinetic Monte Carlo Study of the Sensitivity of OLED Efficiency and Lifetime to Materials Parameters". In: *Advanced Functional Materials* 25.13 (2015), pp. 2024–2037. ISSN: 16163028. DOI: 10.1002/adfm.201402532.

[39] R. Coehoorn, P. A. Bobbert and H. Van Eersel. "Effect of exciton diffusion on the triplet-triplet annihilation rate in organic semiconductor host-guest systems". In: *Physical Review B* 99.2 (Jan. 2019), p. 24201. ISSN: 24699969. DOI: 10.1103/PhysRevB.99.024201.

[40] https://simbeyond.com. The BUMBLEBEE software is provided by Simbeyond B.V.

[41] Simon Zeder et al. "Coupled 3d master equation and 1d drift-diffusion approach for advanced oled modeling". In: *Digest of Technical Papers - SID International Symposium* 51.1 (2020), pp. 2067–2070. ISSN: 21680159. DOI: 10.1002/sdtp.14327.

[42] Weifeng Zhou, Christoph Zimmermann and Christoph A. Jungemann. "Simulation of exciton effects in OLEDs based on the master equation". In: *Organic Light Emitting Materials and Devices XXI*. Vol. 10362. International Society for Optics and Photonics. 2017, p. 63. ISBN: 9781510611818. DOI: 10.1117/12.2269972.

[43] Feilong Liu et al. "Three-Dimensional Modeling of Bipolar Charge-Carrier Transport and Recombination in Disordered Organic Semiconductor Devices at Low Voltages". In: *Physical Review Applied* 10.5 (2018), p. 54007. ISSN: 23317019. DOI: 10.1103/PhysRevApplied.10.054007.

[44] A. V. Shumilin and Y. M. Beltukov. "System of correlation kinetic equations and the generalized equivalent circuit for hopping transport". In: *Physical Review B* 100.1 (2019), p. 14202. ISSN: 24699969. DOI: 10.1103/PhysRevB.100.014202.

[45] Max Born and Herbert S Green. "A general kinetic theory of liquids I. The molecular distribution functions". In: *Proceedings of the Royal Society of London. Series A. Mathematical and Physical Sciences* 188.1012 (1946), pp. 10–18. DOI: 10.1098/rspa.1946.0093.

[46] Nikolai N Bogoliubov. "Kinetic equations". In: *Journal of Physics USSR* 10.3 (1946), pp. 265–274.

[47] John G. Kirkwood. "The statistical mechanical theory of transport processes I. general theory". In: *The Journal of Chemical Physics* 14.3 (Mar. 1946), pp. 180–201. ISSN: 00219606. DOI: 10.1063/1.1724117.

[48] J Yvon. *La Théorie Statistique des Fluides et l'Équation d'Etat, Actualités Scientifiques et Industrialles*. Vol. 203. Hermann & cie, 1935.

[49] Seogjoo Jang, Kook Joe Shin and Sangyoub Lee. "Effects of excitation migration and translational diffusion in the luminescence quenching dynamics". In: *The Journal of Chemical Physics* 102.2 (1995), pp. 815–827. ISSN: 00219606. DOI: 10.1063/1.469196.

[50] Chang Yun Son et al. "An accurate expression for the rates of diffusion-influenced bimolecular reactions with long-range reactivity". In: *Journal of Chemical Physics* 138.16 (2013), p. 164123. ISSN: 00219606. DOI: 10.1063/1.4802584.

[51] Kyusup Lee et al. "Effects of external electric field and anisotropic long-range reactivity on charge separation probability". In: *Journal of Chemical Physics* 147.14 (2017), p. 144111. ISSN: 00219606. DOI: 10.1063/1.5000882.

[52] R. Coehoorn et al. "Effect of polaron diffusion on exciton-polaron quenching in disordered organic semiconductors". In: *Physical Review B* 95.13 (2017), p. 134202. ISSN: 24699969. DOI: 10.1103/PhysRevB.95.134202.

[53] John G. Kirkwood. "Statistical mechanics of fluid mixtures". In: *The Journal of Chemical Physics* 3.5 (1935), pp. 300–313. ISSN: 00219606. DOI: 10.1063/1.1749657.

[54] Inc. Wolfram Research. *Mathematica, Version 12.1*. Champaign, IL, 2020.

[55] Xander de Vries, Reinder Coehoorn and Peter A. Bobbert. "High energy acceptor states strongly enhance exciton transfer between metal organic phosphorescent dyes". In: *Nature Communications* 11.1 (2020), pp. 1–8. ISSN: 20411723. DOI: 10.1038/s41467-020-15034-0.

[56] L. Zhang et al. "Analysis of the phosphorescent dye concentration dependence of triplet-triplet annihilation in organic host-guest systems". In: *Chemical Physics Letters* 662 (2016), pp. 221–227. ISSN: 00092614. DOI: 10.1016/j.cplett.2016.07.048.

[57] Shelden M. Ross. *Introduction to probability models*. twelfth. Academic Press, London, 2019. ISBN: 978-0-12-814346-9.

[58] John G Kirkwood and Elizabeth Monroe Boggs. "The radial distribution function in liquids". In: *The Journal of Chemical Physics* 10.6 (1942), pp. 394–402.

[59] Xander de Vries et al. "Supplemental Material:Triplet exciton diffusion in metal-organic phosphorescent host-guest systems fromfirst-principles". In: *Physical Review B* 99.20 (2019).

[60] Christian Kuehn. "Moment closure—a brief review". In: *Control of self-organizing nonlinear systems* (2016), pp. 253–271.

[61] G. H.A. Cole. "Classical fluids and the superposition approximation". In: *Reports on Progress in Physics* 31.2 (1968), pp. 419–470. ISSN: 00344885. DOI: 10.1088/0034-4885/31/2/301.

[62] Stuart A Rice and John Lekner. "On the equation of state of the rigid-sphere fluid". In: *The Journal of Chemical Physics* 42.10 (1965), pp. 3559–3565.

[63] A. Singer. "Maximum entropy formulation of the Kirkwood superposition approximation". In: *Journal of Chemical Physics* 121.8 (2004), pp. 3657–3666. ISSN: 00219606. DOI: 10.1063/1.1776552.

[64] E. Engel, K. Leo and M. Hoffmann. "Ultrafast relaxation and exciton-exciton annihilation in PTCDA thin films at high excitation densities". In: *Chemical Physics* 325.1 (2006), pp. 170–177. ISSN: 03010104. DOI: 10.1016/j.chemphys.2005.09.004.

[65] Toshiya Yonehara et al. "Comparison of transient state and steady state exciton-exciton annihilation rates based on Förster-type energy transfer". In: *Japanese Journal of Applied Physics* 54.7 (2015), p. 71601. ISSN: 13474065. DOI: 10.7567/JJAP.54.071601.

[66] Tao Pang. *An Introduction to Computational Physics*. second. Cambridge University Press, 2006. ISBN: 978-0-521-53276-1.

[67] Pauli Virtanen et al. "SciPy 1.0: fundamental algorithms for scientific computing in Python". In: *Nature Methods* 17.3 (2020), pp. 261–272. ISSN: 15487105. DOI: 10.1038/s41592-019-0686-2. arXiv: 1907.10121.

[68] G. Peter Lepage. "Adaptive multidimensional integration: VEGAS enhanced". In: *Journal of Computational Physics* 439 (2021), p. 110386. ISSN: 10902716. DOI: 10.1016/j.jcp.2021.110386. arXiv: 2009.05112.

[69] Peter Lepage. "gplepage/vegas: vegas version 4.0.1". Version v4.0.1. In: (May 2021). DOI: 10.5281/zenodo.4746454. URL: https://doi.org/10.5281/zenodo.4746454.

[70] Stan E. A. Jaspers. "Spectro-electrochemical determination of Förster radii for TPQ processes in materials for OLEDs". MA thesis. Technische Universiteit Eindhoven, Mar. 2021.

[71] Andrew C. Fowler. *Notes on statistical mechanics*. https://courses.maths.ox.ac.uk/node/download_material/53410. Jan. 2021.

[72] Pierre-Henri Chavanis. "Generalized stochastic Fokker-Planck equations". In: *Entropy* 17.5 (2015), pp. 3205–3252.

[73] R. Coehoorn, P. A. Bobbert and H. Van Eersel. "Förster-type triplet-polaron quenching in disordered organic semiconductors". In: *Physical Review B* 96.18 (2017), p. 184203. ISSN: 24699969. DOI: 10.1103/PhysRevB.96.184203.

[74] P. Robin Butler and Michael J. Pilling. "The breakdown of Förster kinetics in low viscosity liquids. An approximate analytical form for the time-dependent rate constant". In: *Chemical Physics* 41.1-2 (1979), pp. 239–243. ISSN: 03010104. DOI: 10.1016/0301-0104(79)80148-2.

[75] U. Gösele et al. "Diffusion and long-range energy transfer". In: *Chemical Physics Letters* 34.3 (1975), pp. 519–522. ISSN: 00092614. DOI: 10.1016/0009-2614(75)85553-9.

[76] T. R. Waite. "Theoretical treatment of the kinetics of diffusion-limited reactions". In: *Physical Review* 107.2 (1957), pp. 463–470. ISSN: 0031899X. DOI: 10.1103/PhysRev.107.463.

[77] Joel Keizer. "Diffusion Effects on Rapid Bimolecular Chemical Reactions". In: *Chemical Reviews* 87.1 (1987), pp. 167–180. ISSN: 15206890. DOI: 10.1021/cr00077a009.

[78] U. K.A. Klein et al. "Theoretical and experimental investigations of combined diffusion and long-range energy transfer". In: *Chemical Physics Letters* 41.1 (1976), pp. 139–142. ISSN: 00092614. DOI: 10.1016/0009-2614(76)85266-9.

[79] M. F. Sykes and J. W. Essam. "Critical percolation probabilities by series methods". In: *Physical Review* 133.1A (Jan. 1964), A310–A315. ISSN: 0031899X. DOI: 10.1103/PhysRev.133.A310.

[80] Il Soo Park et al. "Modeling and simulation of electronic and excitonic emission properties in organic host-guest systems". In: *Organic Electronics* 11.2 (2010), pp. 218–226. ISSN: 15661199. DOI: 10.1016/j.orgel.2009.10.020.

[81] Arnout Ligthart et al. "Mechanistic description of the efficiency loss in organic phosphorescent host–guest systems due to triplet-polaron quenching". In: *Organic Electronics* 91 (2021), p. 106058. ISSN: 1566-1199. DOI: https://doi.org/10.1016/j.orgel.2020.106058. URL: https://www.sciencedirect.com/science/article/pii/S1566119920304468.

[82] Mohammad Amir Bazrafshan, Mehdi Ansari-Rad and Saeid Hessami Pilehrood. "Effect of energetic disorder on triplet-triplet annihilation in organic semiconductors". In: *Physical Review B* 101.9 (2020), p. 94204. ISSN: 24699969. DOI: 10.1103/PhysRevB.101.094204.

[83] Oleksandr V. Mikhnenko, Paul W.M. Blom and Thuc Quyen Nguyen. "Exciton diffusion in organic semiconductors". In: *Energy and Environmental Science* 8.7 (2015), pp. 1867–1888. ISSN: 17545706. DOI: 10.1039/c5ee00925a.

[84] Markus Krammer. "Charge Transport in Organic Semiconductor Devices". PhD thesis. Graz: Graz University of Technology, 2019.

[85] Monirul Hasan et al. "Exciton–Exciton Annihilation in Thermally Activated Delayed Fluorescence Emitter". In: *Advanced Functional Materials* 30.30 (2020), p. 2000580. ISSN: 16163028. DOI: 10.1002/adfm.202000580.

[86] GAH Wetzelaer et al. "Trap-assisted and Langevin-type recombination in organic light-emitting diodes". In: *Physical Review B* 83.16 (2011), p. 165204.

[87] J. J.M. Van Der Holst et al. "Electron-hole recombination in disordered organic semiconductors: Validity of the Langevin formula". In: *Physical Review B - Condensed Matter and Materials Physics* 80.23 (2009), p. 235202. ISSN: 10980121. DOI: 10.1103/PhysRevB.80.235202.

[88] A. Blumen and J. Manz. "On the concentration and time dependence of the energy transfer to randomly distributed acceptors". In: *The Journal of Chemical Physics* 71.11 (1979), pp. 4694–4702. ISSN: 00219606. DOI: 10.1063/1.438253.

[89] Joseph R. Lakowicz, Henryk Szmacinski and Michael L. Johnson. "Deviation from the Forster theory for time-dependent donor decays for randomly distributed molecules in solution". In: *Time-Resolved Laser Spectroscopy in Biochemistry II*. Vol. 1204. International Society for Optics and Photonics. 1990, p. 548. ISBN: 0819402451. DOI: 10.1117/12.17747.

[90] Masao Doi. *Soft matter physics*. Oxford University Press, 2013. ISBN: 978-0199652952.

A. Additional NCC & PA formulas

In chapter 2 multiple closures were discussed from which analytical formulas were derived. Not all formulas derived were important enough to present in the main text. These extra formulas will be presented here.

In section 2.4 we neglected to present the entire Master equation and will be presented here. For the system modelled there, the Master equation has become

$$\begin{aligned}
\frac{dP\left(n_1,\ldots,n_N,t\right)}{dt} = \sum_{i,j\neq i}[&-W_{ij}^{TTA}n_{i,T}n_{j,T}P(n_1,\ldots,n_N,t) + W_{ij}^{TTA}n_{i,T}(1-n_{j,T})P(n_1,\ldots,n_{j,T}+1,\ldots,n_N,t)\\
&- W_{ij}^{TPQ}n_{i,P}n_{j,T}P(n_1,\ldots,n_N,t) + W_{ij}^{TPQ}n_{i,P}(1-n_{j,T})P(n_1,\ldots,n_{j,T}+1,\ldots,n_N,t)\\
&+ D_{ij}^{TT}n_{j,T}(1-n_{i,T})(1-n_{i,P})(1-n_{j,P})P(n_1,\ldots,n_{i,T}+1,\ldots,n_{j,T}-1,\ldots,n_N,t)\\
&- D_{ij}^{TT}n_{i,T}(1-n_{j,T})(1-n_{j,P})(1-n_{i,P})P(n_1,\ldots,n_N,t)\\
&+ D_{ij}^{PP}n_{j,P}(1-n_{i,P})(1-n_{i,T})(1-n_{j,T})P(n_1,\ldots,n_{i,P}+1,\ldots,n_{j,P}-1,\ldots,n_N,t)\\
&- D_{ij}^{PP}n_{i,P}(1-n_{i,T})(1-n_{j,P})(1-n_{j,T})P(n_1,\ldots,n_N,t)]\\
&+ \sum_i[-k_r n_{i,T}P(n_1,\ldots,n_N,t) + k_r(1-n_{i,T})P(n_1,\ldots,n_{i,T}+1,\ldots,n_N,t)\\
&+ Gn_{i,T}(1-n_{i,P})P(n_1,\ldots,n_{i,T}-1,\ldots,n_N,t) - G(1-n_{i,T})(1-n_{i,P})P(n_1,\ldots,n_N,t)],
\end{aligned} \tag{A.1}$$

where in lines 2, 5 and 6 TPQ and diffusion of polarons were added respectively. Lines 3, 4 and 8 were altered to account for the fact that excitons cannot be present on a site with a polaron.

As noted the first order NCC closure denotes the solution for strongly diffusing excitons. The general solution of the first order NCC equation was presnted in equation (2.19). This equation consists of the TTA rate coefficient k_{TTA}. In the text this parameter was merely derived for Förster-type TTA in 3 spatial dimensions. For general spatial dimensions $d < 6$ one obtains for Förster-type TTA

$$k_{TTA} = 2\frac{2\pi^{d/2}k_r R_{F,TTA}^6}{(6-d)\,\Gamma\left(d/2\right)R_0^{6-d}}. \tag{A.2}$$

For Dexter-type TTA for any general spatial dimensions d for strongly diffusing excitons this turns into

$$k_{TTA} = 2\frac{2^{1-2d}\pi^{d/2}k_{Dex}^{TTA}\lambda_{TTA}^d\Gamma\left(d,\frac{12R_0}{\lambda_{TTA}}\right)}{3^d\Gamma\left(d/2\right)}. \tag{A.3}$$

During the derivations of the analytical formulas for the PA closures we have always assumed $R_0 = 0$, since that assumption generally does not cause a significant deviation from the actual results as noted in Ref. [49]. It has however been noted that in certain scenarios this parameter can contribute significantly [88, 89]. We can rewrite equation (2.26) in three spatial dimensions for $R_0 > 0$ as

$$n_T(t) = 3n_0 e^{-k_r t}\left\{\pi^2\sqrt{2}n_0 R_{F,TTA}^3\left[4T\left(\frac{2R_{F,TTA}^3\sqrt{k_r t}}{R_0^3}, \frac{R_0^3}{\sqrt{2}R_{F,TTA}^3}\right)\right.\right. \\ \left.\left. + \operatorname{erf}\left(\sqrt{k_r t}\right)\operatorname{erf}\left(\frac{\sqrt{2}R_{F,TTA}^3\sqrt{k_r t}}{R_0^3}\right) - \frac{2}{\pi}\arctan\left(\frac{R_0^3}{\sqrt{2}R_{F,TTA}^3}\right)\right] + 3\right\}^{-1}, \tag{A.4}$$

where $T(a,x)$ denotes Owen's T function. Here we conclude that we can set $R_0 = 0$ without mayor errors when both $R_0^3 \ll R_{F,TTA}^3$ and $R_0^3 \ll R_{F,TTA}^3\sqrt{k_r t}$. We can also do this to the steady state originally given in equation (2.29) yielding

$$Gn_{max} = \frac{2}{3}\pi R_{F,TTA}^3 n_T\sqrt{Gk_r n_{max} n_T}\left[\pi - 2\arctan\left(\frac{R_0^3}{R_{F,TTA}^3}\sqrt{\frac{Gn_{max}}{k_r n_T}}\right)\right] + (G + k_r)n_T. \tag{A.5}$$

From the two equations above we can conclude that for the formulas presented in the main text are accurate when $R_0^3 \ll R_{F,TTA}^3\sqrt{\frac{k_r n_T(G)}{Gn_{max}}}$.

We can also derive the steady state equation using the PA closure (equation (2.29)) with Dexter-type TTA. The solution is then for any general dimensionality d

$$Gn_{max} = \frac{2(-1)^d\pi^{d/2}G\lambda^d n_{max}\Gamma(d)n_T\mathrm{Li}_d\left(-\frac{k_{Dex}^{TTA}n_T}{Gn_{max}}\right)}{\Gamma\left(\frac{d}{2}\right)} + (G + k_r)\,n_T, \tag{A.6}$$

where $\mathrm{Li}_d(x)$ denotes the polylogarithm function.

Now moving on to the TPQ problem. For a system without TTA nor any diffusion with $R_0 > 0$ during a TRPL experiment for any general dimensionality d

$$n_T(t) = n_0\exp\left\{\pi^{d/2}n_P\left[R_0^d\left(1 - e^{-\frac{R_{F,TPQ}^6 k_r t}{R_0^6}}\right) - R_{F,TPQ}^d(k_r t)^{d/6}\,\gamma\left(1 - \frac{d}{6}, \frac{R_{F,TPQ}^6 k_r t}{R_0^6}\right)\right]/\Gamma\left(\frac{d}{2}+1\right) - k_r t\right\}. \tag{A.7}$$

We can furthermore rewrite equation (2.47), which denotes the steady state for non-diffusing particles, for any general dimensionality d as

$$\frac{\pi^{\frac{d}{2}+1}Gn_T\left(n_{max}R_{F,TTA}^d\left(R_{F,TTA}^6 - R_{F,TPQ}^6\right) + n_P R_{F,TTA}^6\left(R_{F,TPQ}^d - R_{F,TTA}^d\right)\right)}{3\sin\left(\frac{\pi d}{6}\right)\Gamma\left(\frac{d}{2}\right)\left(R_{F,TTA}^6 - R_{F,TPQ}^6\right)\left(\frac{G(n_{max}-n_P)}{k_r n_T}\right)^{\frac{d}{6}}} \\ + \frac{\pi^{\frac{d}{2}+1}k_r n_P n_T R_{F,TPQ}^d\left(\frac{G(n_{max}-n_P)}{k_r n_T}\right)^{1-\frac{d}{6}}}{3\sin\left(\frac{\pi d}{6}\right)\Gamma\left(\frac{d}{2}\right)} = G(n_{max} - n_P - n_T) - k_r n_T \tag{A.8}$$

The last two equations will be related to the system with both TTA and TPQ for strongly diffusing polarons, but perfectly confined excitons for any spatial dimensionality d. The TRPL experiment is given by

$$
\begin{aligned}
n_T(t) = 36 n_0 \Gamma\left(\frac{d}{2}\right)\left(1 - \frac{2\pi^{d/2} n_P R_{F,TPQ}^6 R_0^{d-6}}{(d-6)\Gamma\left(\frac{d}{2}\right)}\right)^{d/6} & e^{k_r t\left(\frac{2\pi^{d/2} n_P R_{F,TPQ}^6 R_0^{d-6}}{(d-6)\Gamma\left(\frac{d}{2}\right)} - 1\right)} \\
\Bigg\{ 36\Gamma\left(\frac{d}{2}\right)\left(1 - \frac{2\pi^{d/2} n_P R_{F,TPQ}^6 R_0^{d-6}}{(d-6)\Gamma\left(\frac{d}{2}\right)}\right)^{d/6} & \\
- 2^{d/6} d \pi^{d/2} n_0 R_{F,TTA}^d \Gamma\left(-\frac{d}{6}\right)\gamma\left(\frac{d}{6}, k_r t\left[1 - \frac{2 n_P \pi^{d/2} R_0^{d-6} R_{F,TPQ}^6}{(d-6)\Gamma\left(\frac{d}{2}\right)}\right]\right)\Bigg\}^{-1}. &
\end{aligned}
\tag{A.9}
$$

Now a system where polarons diffuse strongly, while excitons are perfectly confined and both TTA and TPQ play a role has the characteristic equation in steady state for any dimensionality d

$$
\frac{\pi^{\frac{d}{2}+1} k_r n_T^2 R_{F,TTA}^d \left(\frac{G\tau(n_{max}-n_P)}{n_T}\right)^{1-\frac{d}{6}}}{3\sin\left(\frac{\pi d}{6}\right)\Gamma\left(\frac{d}{2}\right)} + \frac{2\pi^{d/2} k_r n_P n_T R_{F,TPQ}^6 R_0^{d-6}}{(6-d)\Gamma\left(\frac{d}{2}\right)} = G(n_{max} - n_P - n_T) - k_r n_T. \tag{A.10}
$$

B. Small percolation study

In chapter 3 it was noted that our original naïve implementation of diffusion did not adequately account for percolation effects. Where our naïve implementation only accounted for the diffusion coefficient to adhere to $D \propto c_{guest}$, in literature it is noted that $D \propto c_{guest}^{4/d}$ for Förster-type hopping, where d denotes the spatial dimensionality. We then proposed an effective lattice method which concluding from (2.54) yields $D \propto c_{guest}^{4/d}$. In section 3.2 it was then noted that our proposed method underestimates diffusion and it seemed that for $c_{guest} \gtrsim 40\%$ the original naive implementation yielded better results when compared to KMC. For this reason we will conduct a small percolation type study to see whether square lattices have an effect. We will focus on the 2D square lattice, since this remains computationally feasible, while still allowing for percolation effects. The main theory has been presented in section 2.5.

In figure B.1 we compare the results of the modelling using equations (2.51) and (2.48) for $R_{F,Diff} = 1$ nm and $k_r = 1\mu\text{s}^{-1}$ with initial condition $n_T(r,0) = n_0\delta(r)$, where $n_0 = 1$ nm^{-2}. The result of equation (2.48) is shown for hopping on a 2D square lattice. The solution of equation (2.51) is here given by

$$n_T(r,t) = n_0 (4\pi D t)^{-d/2} e^{-\frac{r^2}{4Dt}}, \tag{B.1}$$

where for Förster-type diffusion on a 2D simple square lattice $D = 1.507 k_r c_{guest}^2 \frac{R_{F,Diff}^6}{a^4}$, where a denotes the square lattice length.

From figure B.1 we can conclude that at long time-scales the methods are alike. This is surprising, since higher order moments of displacement explode as noted in equation (2.52). We would have expected the particles to diffuse faster than the Fick's second law indicates. Nevertheless since the diffusion coefficients are alike at large times the results are equal, since the underlying lattice is not felt. At short times the results are different due to the underlying lattice. Note that the Förster-hopping theory here yields a linear increase in time, as would be expected from equation (2.48), due to the discrete lattice. The results from Fick's second law show a different dependency, due to being related to Brownian motion in continuum.

Due to the results being equal at long times, we can calculate the dependency of the diffusion coefficient on percentage of guest molecules in the system. From the Fickian theory it has been noted that the diffusion coefficient is equal to $D = \frac{\langle r^2 \rangle(t)}{2dt}$ [90]. We will use this relation for determining the dependency of D on c_{guest} within the theory of equation (2.48).

The diffusion coefficent as calculated above as a function of guest percentage is shown in figure B.2. It is clear that the diffusion coefficient D is lowered with lower c_{guest}. The simulated data is very noisy, thus conclusions will be to some extent refutable. It is however clear that the lowest values found quite perfectly are related to $D \propto c_{guest}^2$. This also seems to hold on average for lower values of c_{guest}. It does seem like that on average when c_{guest} is near 100% that $D \propto c_{guest}^{\gamma}$ with $1 \leq \gamma \leq 2$. This also corresponds to what was found above. Thus percolation effects might cause the effective lattice approach to fall short in terms of diffusion strength. We do need to account for the fact that we might not have simulated this system for large enough times, especially at low c_{guest}. This might cause deviations from the actual result.

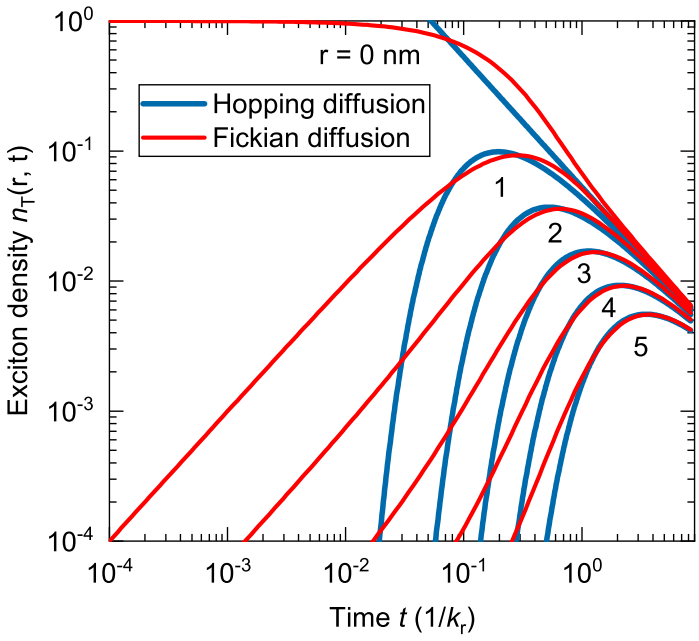

Figure B.1: Exciton density $n_T(r,t)$ as a response to initial condition $n_T(r,0) = n_0\delta(r)$, where $n_0 = 1$ nm^{-2} on a 2D simple square lattice for the equations (2.51) (blue) and (2.48) (red). Here the hopping is assumed to be of Förster-type, given by equation (1.4). The diffusion constant D is then given by $1.507k_r c_{guest}^2 \frac{R_{F,Diff}^6}{a^4}$. Here $R_{F,Diff} = 1$ nm and $k_r = 1\mu s^{-1}$ for simplicity.

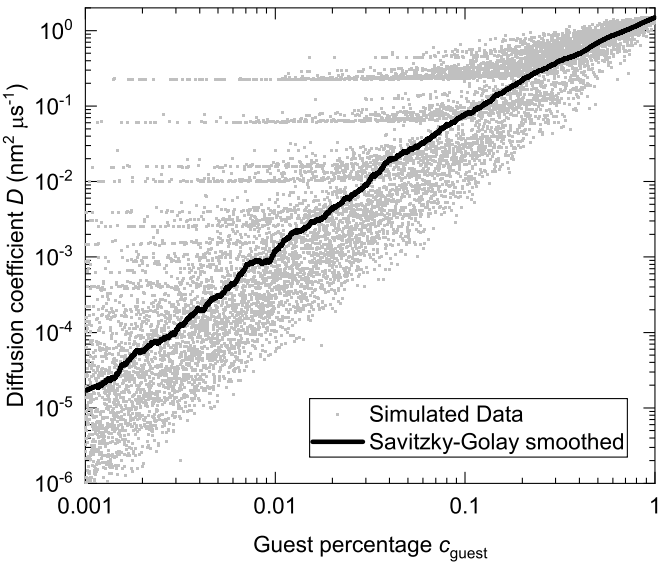

Figure B.2: Diffusion coefficient D as a function of guest percentage c_{guest}. This is calculated from the theory presented in equation (2.48) with initial condition $n_T(r,0) = n_0\delta(r)$, where $n_0 = 1$ nm^{-2} on a 2D simple square lattice. The hopping is assumed to be of Förster-type, given by equation (1.4). The parameters are set as $R_{F,Diff} = 1$ nm and $k_r = 1\mu s^{-1}$ for simplicity. The diffusion constant is then calculated as $D = \frac{\langle r^2\rangle(t)}{2dt}$. The simulated data is presented as well as the smoothed data using the Savitzky-Golay filter.